1   **African Smoke Particles Act as Cloud Condensation Nuclei in the Wintertime Tropical**

2   **North Atlantic Boundary Layer over Barbados**

3   Haley M. Royer[1], Mira L. Pöhlker[2,3,4*], Ovid Krüger[2], Edmund Blades[5,6], Peter Sealy[5], Nurun

4   Nahar Lata[7], Zezhen Cheng[7], Swarup China[7], Andrew P. Ault[8], Patricia K. Quinn[9], Paquita

5   Zuidema[1], Christopher Pöhlker[2], Ulrich Pöschl[2], Meinrat Andreae[2,10,11] and Cassandra J.

6   Gaston[1*]

7   [1]Department of Atmospheric Sciences, Rosenstiel School of Marine, Atmospheric, and Earth

8   Science, University of Miami, Miami, FL

9   [2]Department of Multiphase Chemistry, Max Planck Institute for Chemistry, Mainz, Germany

10   [3]Leipzig Institute for Meteorology, Leipzig University, Leipzig, Germany

11   [4]Experimental Aerosol and Cloud Microphysics Department, Leibniz Institute for Tropospheric

12   Research, Leipzig, Germany

13   [5]Barbados Atmospheric Chemistry Observatory, Ragged Point, Barbados

14   [6]Queen Elizabeth Hospital Barbados, Bridgetown, Barbados

15   [7]Environmental Molecular Sciences Laboratory, Pacific Northwest National Laboratory,

16   Richland, WA

17   [8]Department of Chemistry, University of Michigan, Ann Arbor, MI

18   [9]Pacific Marine Environmental Laboratory, National Oceanic and Atmospheric Administration,

19   Seattle, WA

20   [10]Department of Geology and Geophysics, King Saud University, Riyadh, Saudi Arabia

21   [11]Scripps Institution of Oceanography, University of California San Diego, La Jolla, California,

22   USA

23   *Corresponding Authors:

24   Mira L. Pöhlker: Email: poehlker@tropos.de, Phone: +49 6131 305 7020

25   Cassandra J. Gaston: Email: cgaston@.miami.edu, Phone: (305)-421-4979

Abstract

The number concentration and properties of aerosol particles serving as cloud condensation nuclei (CCN) are important for understanding cloud properties, including in the tropical Atlantic marine boundary layer (MBL) where marine cumulus clouds reflect incoming solar radiation and obscure the low-albedo ocean surface. Studies linking aerosol source, composition, and water uptake properties in this region have been conducted primarily during the summertime dust transport season, despite the region receiving a variety of aerosol particle types throughout the year. In this study, we compare size-resolved aerosol chemical composition data to the hygroscopicity parameter κ derived from size-resolved CCN measurements made during the EUREC[4]A and ATOMIC campaigns from January to February 2020. We observed unexpected periods of wintertime long-range transport of African smoke and dust to Barbados. During these periods, the accumulation mode aerosol particle and CCN number concentrations as well as the proportions of dust and smoke particles increased, whereas the average κ slightly decreased (κ = 0.46 ± 0.10) from marine background conditions (κ = 0.52 ± 0.09) when the particles were mostly composed of marine organics and sulfate. Size-resolved chemical analysis shows that smoke particles were the major contributor to the accumulation mode during long-range transport events, indicating that smoke is mainly responsible for the observed increase in CCN number concentrations. Earlier studies conducted at Barbados have mostly focused on the role of dust on CCN, but our results show that aerosol hygroscopicity and CCN number concentrations during wintertime long-range transport events over the tropical North Atlantic are also affected by African smoke. Our findings highlight the importance of African smoke for atmospheric processes and cloud formation over the Caribbean.

Introduction

Aerosol particle number, size, hygroscopicity, and chemical mixing state determine cloud droplet formation and, thus, fundamentally affect the radiative properties and lifetime of clouds (Albrecht, 1989; McFiggans et al., 2006; Quinn et al., 2008; Twomey, 1977; Zuidema et al., 2008). Quantifying the effect of aerosols on cloud radiative forcing, however, is still the single largest source of uncertainty in predicting temperature increases associated with climate change (Forster et al., 2021). This uncertainty is especially important to resolve in marine regions where aerosol-cloud interactions are understudied, even though the majority of Earth's surface is covered by oceans (Carslaw et al., 2013). The existing literature that explores marine aerosol-cloud interactions does so primarily in the mid to high latitudes of the North Atlantic with few studies focusing in tropical latitudes where shallow cumulus clouds form (Allan et al., 2008; Behrenfeld et al., 2019; Klingebiel et al., 2019; Rauber et al., 2007; Sorooshian et al., 2020). Shallow cumulus clouds are important for Earth's climate as they are one of the most geographically pervasive cloud types and can influence Earth's radiative budget by reflecting incoming radiation over the low-albedo ocean surface.

Aerosol research conducted in the tropical Atlantic has focused largely on the long-range transport of mineral dust from North Africa in the summertime. Long-range African dust transport occurs when emitted desert dust is lofted above the marine boundary layer (MBL) into the Saharan Air Layer (SAL) and is propagated westward (Carlson & Prospero, 1972). As dust is transported westward, it can mix into the underlying moist MBL and deposit into the Atlantic Ocean and Caribbean Sea as well as Western Atlantic land masses such as South America, the Caribbean islands, and North America (Barkley et al., 2019; Carlson & Prospero, 1972; Prospero et al., 1981, 2020). Some studies have attempted to understand the effects of long-range transported

74 dust on cloud droplet formation and water uptake with varying results depending on the degree

75 of aging that dust experiences during transport (Allan et al., 2008; Denjean et al., 2015;

76 Kristensen et al., 2016; Rosenfeld et al., 2001; Wex et al., 2016). However, these studies provide

77 conflicting results on whether dust particles are hygroscopic and numerous enough to

78 appreciably impact CCN concentrations in the tropical Atlantic. Due to the annual oscillation of

79 the intertropical convergence zone (ITCZ), dust transport also exhibits a seasonality in terms of

80 its geographic extent (Adams et al., 2012; Chin et al., 2014; Prospero & Lamb., 2003; Prospero, 1968;

81 Prospero & Mayol-Bracero, 2013; Yu et al., 2019; Zuidema et al., 2019). However, marine shallow

82 cumulus clouds form year-round in the tropical Atlantic regardless of dust transport. Thus, it is

83 important to focus on aerosol characteristics across a full seasonal cycle to obtain a thorough

84 understanding of the role aerosols play on cloud formation in the tropical Atlantic (McCoy et al.,

85 2022).

86   Few studies have attempted to fully understand which aerosols are the most prominent

87 CCN during both the boreal summer (when dust concentrations are at a maximum) and boreal

88 winter (when dust concentrations are at a minimum) in the tropical North Atlantic MBL. African

89 smoke is one particle type that may be important for CCN activation in the tropical North

90 Atlantic, yet has been understudied at dust receptor sites like Barbados (Wex et al., 2016). In

91 contrast to dust, previous research has shown that smoke particles are an important source of

92 CCN (Edwards et al., 2021; Lathem et al., 2013; Pierce et al., 2007; Spracklen et al., 2011) with

93 some research showing that smoke particles can activate at supersaturations as low as 0.05%

94 (Rogers et al., 1991).

95   There are a number of reasons that explain why smoke particles can be effective CCN.

96 Smoke particles are often complex mixtures of both organic and inorganic components that

97   change compositionally and morphologically during their residence time in the atmosphere

98   (Cappa et al., 2020; Hodshire et al., 2019; Konovalov et al., 2021; Reid et al., 2005; Wu et al.,

99   2021). Smoke properties may also vary between fires depending on fuel type and moisture,

100   combustion phase, wind conditions, etc. (Andreae, 2019; Miles et al., 1995; Reid et al., 2005). In

101   general, smoke particles are often found in the accumulation mode of the aerosol size

102   distribution and primarily contain particulate organic matter, black carbon, and inorganic

103   components including potassium chloride salts (Reid et al., 2005). Upon emission, smoke can

104   undergo chemical processing through photochemical and heterogeneous reactions, including the

105   loss of chloride and acquisition of sulfate and nitrate, creating potassium sulfate compounds in

106   smoke that are often used as tracers of aged smoke and can affect the hygroscopicity of smoke

107   particles (Capes et al., 2008; Hennigan et al., 2010, 2011; Reid et al., 2005; Zauscher et al.,

108   2013). Chemical processing can also lead to morphological changes as the condensation of

109   gaseous compounds and multiphase processes with aqueous compounds can result in the growth

110   and sphericity of smoke particles, which in turn can affect the CCN properties of smoke particles

111   (Abel et al., 2003; Giordano et al., 2015; Reid et al., 1998; Zhang et al., 2008). The variations in

112   the chemical and physical properties of emitted smoke particles as well as the changes these

113   properties can undergo in transit make it difficult to predict the ability of smoke particles to act

114   as CCN.

115   In this study, we investigated the relationship between submicron aerosol composition

116   and CCN in the tropical North Atlantic MBL during marine background conditions and

117   conditions affected by long-range continental aerosol transport of smoke and dust particles

118   (henceforth referred to as "CAT" conditions). To perform this work, we collected aerosol

119   samples and size-resolved CCN data from January to February 2020 at the Barbados

Atmospheric Chemistry Observatory (BACO) during the Elucidating the Role of Clouds–

Circulation Coupling in Climate/Atlantic Tradewind Ocean-Atmosphere Mesoscale Interaction

Campaign (EUREC^{4}A/ATOMIC) campaigns (Quinn et al., 2021; Stevens et al., 2021).

Conducting this research during the boreal winter provided a unique opportunity to explore

aerosol-cloud interactions in meteorological conditions different from those that are typically

studied in the tropical North Atlantic. Dust primarily arrives to Barbados during the summer

months with peaks in June and July (Zuidema et al., 2019). As a result, dust receptor sites in

Barbados have historically been used to compare CAT and marine background conditions during

the boreal summer. During the winter, the southward shift of the ITCZ directs African dust to

South America, resulting in a decrease in dust concentrations over Barbados during the winter

months with days in December and January sometimes receiving no dust at all (Prospero, 1968;

Prospero et al., 2014; Prospero & Lamb, 2003; Prospero & Mayol-Bracero, 2013). However, during the

EUREC^{4}A/ATOMIC campaigns, we observed anomalous wintertime transport of African

aerosols to Barbados, which provided novel sampling conditions to study the effects of various

aerosol types on cloud droplet formation. Specifically, we were able to explore how the addition

of continental aerosols like mineral dust and smoke particles to background marine aerosols

consisting of organics, sulfates, and sea salt affects CCN activity. This allowed us to compare the

impact of ocean-derived vs. long-range transported aerosol on water uptake properties and CCN

concentrations. We conclude this manuscript by discussing the importance of our findings for

cloud formation in the tropical North Atlantic.

Methods

Measurement Site and Sampling Period

142   Aerosol samples and size-resolved CCN data were collected at the Barbados

143   Atmospheric Chemistry Observatory (BACO) on Ragged Point during the EUREC[4]A and

144   ATOMIC field campaigns from January 20, 2020 -February 20, 2020 (Quinn et al., 2021;

145   Stevens et al., 2021). Ragged Point (13° 6' N, 59° 37' W), a prominence on Barbados' east coast,

146   is an ideal location for studying the impact of long-range African aerosol transport on aerosol-

147   cloud interactions as it is situated on the most easterly island in the Caribbean and is exposed to

148   the steady easterly trade winds. Thus, the east coast of the island is subject to little anthropogenic

149   aerosol influence from local islands to the west (Prospero et al., 2005; Savoie et al., 2002).

150   Further, the island is at a latitude coinciding with the outflow of African aerosols such as mineral

151   dust (Carlson & Prospero, 1972; Prospero, 1968) and smoke particles (Archibald et al., 2015) as well

152   as tropical marine cumulus clouds (Stevens et al., 2016).

153   Air Mass Origins

154   During the sampling period, air masses of varying compositions were observed at Ragged

155   Point. To determine the origin of these air masses, 150 h back trajectories were generated every 6

156   h at heights of 500, 1000, and 1500 m throughout the campaign using the NOAA Hybrid Single

157   Particle Lagrangian Integrated Trajectory (HYSPLIT) model calculated using model vertical

158   velocity and meteorology from the National Center for Environmental Prediction (NCEP) 1-

159   degree Global Data Assimilation System (GDAS) (Rolph et al., 2017; Stein et al., 2015).

160   Dust Concentration

161   To collect aerosols, BACO is equipped with a high-volume sampler and an isokinetic

162   aerosol inlet on top of a 17 m tall tower situated on a 30 m bluff along the coast at Ragged Point.

163   Daily dust mass concentrations were determined from filter-based measurements (Prospero et al.,

164 2021; Zuidema et al., 2019) using a high-volume air sampler pumping at a rate of approximately

165 0.7 m^3/min across a 20 cm x 25 cm cellulose Whatman-41 (W-41) filter with a nominal 20 μm

166 pore size. W-41 filters were chosen for this analysis as they allow high flow rates and yield a

167 collection efficiency of 95% or better for dust (Kitto & Anderson, 1988) and submicron aerosols

168 (Pszenny et al., 1993). Upper particle diameter limits for W-41 filters are approximately 80-100

169 μm or greater (Barkley et al., 2021). After aerosol collection, the filters are washed with milli-q

170 water three times to remove soluble material then placed in a furnace and combusted at 500°C

171 for about 12 h (i.e., overnight). Procedural blanks are also collected by placing a filter in the

172 sampler for 15 minutes without turning on the pump. The resulting ash mass from a sample

173 minus the mass of a filter blank is the gross ash weight, which is then adjusted by a factor of 1.3

174 to convert the ash weight to a mineral dust concentration. Previous research has confirmed the

175 validity of this method for determining dust mass concentrations through chemical analysis of

176 dust ash determined from filters collected in Barbados, crustal abundance, and soil dust

177 composition (Zuidema et al., 2019). A correction factor of 1.3 is applied to the calculated dust

178 concentrations to account for dust components such as bound water or soluble ions that are lost

179 during the heating process (Prospero, 1999; Zuidema et al., 2019).

180 Aerosol Chemical Composition

181 Aerosol particles were sampled at ambient relative humidity (RH) through an isokinetic

182 aerosol inlet and collected using a three-stage microanalysis particle sampler (MPS-3, California

183 Measurements, Inc.), which samples particles from diameters of 5.0-2.5 μm (stage 1), 2.5 μm –

184 0.7 μm (stage 2), and <0.7 μm (stage 3). For each set of samples (1 set including 1 sample from

185 each stage of the MPS), the MPS was run for 45 min at 2 L/min flow starting at approximately

186 9:30 local time or 13:30 coordinated universal time (UTC). Meteorological data from a local

187   station was also used to manually check that wind direction fell between 335° and 130° and wind

188   speeds were greater than 1 m/s during all sampling periods. Sampling during these wind

189   conditions ensures that only air from the open ocean was sampled rather than local,

190   anthropogenically-influenced air.

191   To determine aerosol chemical composition, particles were deposited onto carbon-

192   coated copper grids (Ted Pella, Inc.) that were later analyzed at the Pacific Northwest National

193   Laboratory using computer-controlled scanning electron microscopy coupled with energy

194   dispersive x-ray spectroscopy (CCSEM/EDX; Quanta 3D) to determine the elemental

195   composition of individual particles. We also collected samples on silicon wafers (Ted Pella, Inc.)

196   which were analyzed with CCSEM/EDX to confirm the vaolidity of the carbon measurements on

197   the carbon-coated copper grids. Here, we focus only on the submicron particle population which

198   exerts a greater influence on CCN number concentrations and is more sensitive to chemical

199   changes that affect its hygroscopicity. Thus, for this study we focus primarily on data from stage

200   3 of the MPS, representing <0.7 μm diameter particles.

201   CCSEM/EDX is a valid method for determining size-resolved chemistry of the aerosol

202   loading as CCSEM excels in calculating particle size by imaging individual aerosols while EDX

203   provides the relative abundances for elements of interest (Tomlin et al., 2021). Percent

204   composition threshold values of 1% were used to ensure the presence of elements detected by the

205   EDX. Single-particle analysis using CCSEM/EDX was limited to 16 elements found in common

206   aerosols such as dust, sea salt, and smoke particles: carbon (C), nitrogen (N), oxygen (O),

207   sodium (Na), magnesium (Mg), aluminum (Al), silicon (Si), phosphorus (P), sulfur (S), chlorine

208   (Cl), potassium (K), calcium (Ca), vanadium (V), manganese (Mn), iron (Fe), and nickel (Ni).

209   The EDX peak for Cu is heavily influenced by the background signal from the Cu grid and is

210 excluded from analysis. Samples collected on Si substrates confirmed the validity of the C signal

211 in analyzed particles, as the carbon coating on the Cu substrates has the potential to generate a

212 background signal as well. An excess of 1000 particles were analyzed in each sample. Due to

213 size limitations of the CCSEM, only particles with diameters >0.1 μm were analyzed. Data

214 products from CCSEM/EDX analysis were then analyzed in MATLAB (ver 9.6.0; The

215 Mathworks, Inc.) using a K-means clustering algorithm (Ault et al., 2012; Shen et al., 2016). The

216 algorithm operates by generating categories of similar particles (clusters) based on the presence

217 and intensity of elemental peaks in individual single-particle EDX spectra. These clusters are

218 then assigned to particle types based on their size, morphology, characteristic EDX spectra, and

219 existing literature. A more thorough explanation of the k-means clustering algorithm and particle

220 identification process including the plots used to perform particle identification (Figure S1) is

221 provided in the Supporting Information (SI).

222 Size-Resolved CCN Measurements and Data Analysis

223 To determine the size-resolved CCN activity of aerosol particles during the sampling

224 period, we used a continuous-flow streamwise thermal gradient CCN counter (CCNC, model

225 CCN-100, DMT, Longmont, Co, USA; (Roberts & Nenes, 2005; Rose et al., 2008)) combined with

226 a differential mobility analyzer (DMA, modified model M, Grimm Aerosol Technik, Ainring,

227 Germany) and condensation particle counter (CPC, model 5412, Grimm Aerosol Technik). The

228 method is described in detail in Pohlker et al. (2016). Flows for the size-resolved CCN set-up

229 included a sheath:sample flow ratio of 10 for the CCN counter (sample flow rate of 0.5 L/min), a

230 sheath flow of 8 L/min for the DMA, and a sample flow of 0.6 L/min for the CPC. Upon entering

231 the system, the sampled air was dried using a condensation drier to maintain a relative humidity

232 (RH) between 20 and 30% and to ensure reliable hygroscopicity measurements. After drying, the

233 particles passed through a DMA which selected particles with a diameter (D) between 20 and

234 245 nm. The monodisperse aerosol-laden flow was then split between the CCNC and CPC.

235 Inside the CCNC, the particles were subjected to supersaturations (S) of 0.09, 0.16, 0.24, 0.43,

236 and 0.74 %.

237   Calibrations of the CCNC supersaturations were performed according to the method

238 described in Rose et al. (2008) by generating and size-selecting ammonium sulfate particles that

239 were analyzed by the CCNC set to a designated temperature gradient as well as a CPC to

240 measure total condensation nuclei (CN) values. Plots comparing CCN/CN and dry particle

241 diameter were then used to determine the diameter at which 50% of the particles in an aerosol

242 population activate as CCN at a particular S, also called the critical activation diameter (d_{50}). D_{50}

243 values were then used to determine supersaturation. Supersaturations were plotted against the

244 designated temperature at the calculated supersaturation. The resulting plot provided a linear

245 curve that could be used to adjust the supersaturation shown by the instrument to the actual value

246 of the column supersaturation. After calibrating, S values averaged 0.08, 0.15, 0.23, 0.41, and

247 0.71%.

248   For ambient sampling, particles that activate as CCN at each S and D are counted in the

249 CCNC as CCN, while all particles of a selected D are counted in the CPC to determine the total

250 aerosol concentration of particles at each D. By scanning D at a given value of S, measurements

251 from the CPC and CCNC are then used to generate an activation curve used to calculate the d_{50}.

252 These values, along with the particle number size distribution determined by an SMPS (SMPS,

253 Grimm model 5420 with CPC 3772) operating independently of the CCNC set-up, are then used

254 to calculate the effective hygroscopicity parameter κ using equation (1) according to the κ-

255 Köhler model (Petters & Kreidenweis, 2007):

256
$$\kappa = \frac{4A^3}{27D_p^3 \ln^2 S_{crit}}$$
(1)

257 where D_p is the dry particle diameter, S_{crit} is the supersaturation set by the CCN counter, and A is

258 the Kelvin term calculated from equation (2):

259
$$A = \frac{4\sigma M_w}{RT\rho_w}$$
(2)

260 Where σ is the surface tension ($\sigma=0.072$ J/m^2), R is the universal gas constant, M_w is the

261 molecular weight of water, and ρ_w is the density of water. In the κ-Köhler model, higher values

262 of κ indicate a more hygroscopic particle that is more efficient at taking up water and can

263 activate as CCN at lower S.

264 **Results and Discussion**

265   In this section we will show that, upon arrival of co-transported dust and smoke, smoke

266 originating from fires in the African Sahel dominate the accumulation mode particle population

267 in the tropical North Atlantic MBL, which results in an increase in CCN number concentration.

268 Though dust and smoke are both transported to the region, smoke dominates the accumulation

269 mode number concentration by an order of magnitude compared to dust. These findings are

270 supported by data products from dust mass concentrations, size-resolved hygroscopicity, single

271 particle data (CCSEM-EDX), and air mass history (NOAA'S HYSPLIT model), which all

272 complement one another and provide unique insights into the aerosol sources, their single

273 particle composition, and their effects on cloud droplet activation.

274 Air Mass Characteristics during the EUREC[4]A and ATOMIC Campaigns

275   To confirm the origins of the various air masses sampled, we performed back trajectory

276 analysis throughout the campaign using NOAA's HYSPLIT model (Figure 1) and quantified

277   dust mass concentrations (Figure 2a). Results of these two analyses show that Barbados was

278   influenced by two types of air masses during the sampling period: air masses that, over the

279   course of 6 days, do not pass over land (referred to as clean marine conditions), and air masses

280   that have passed over the African continent (referred to as continental aerosol transport (CAT)

281   events). Back trajectory analysis was not conducted for time periods longer than 6 days, which

282   introduces the possibility that marine air masses could have been influenced by European

283   outflow as well. Figure 1 shows that during periods with low dust mass concentrations and a

284   bimodal size distribution, air masses originated from the remote Atlantic Ocean at higher

285   latitudes with no land contact over 6 days. During time periods with high dust mass

286   concentrations, air masses originated from continental Africa. Figure 2a shows that the total

287   mass concentration of dust particles correlates very well with the arrival of air masses originating

288   from Africa. During time periods when dust concentrations were low, the particle loading has a

289   bimodal size distribution characteristic of clean marine air masses (Figure 2b; Ault et al., 2013;

290   Hoppel et al., 1986; O'Dowd et al., 2004). Upon the increase in dust mass concentrations, the

291   submicron particle size distribution becomes unimodal and the smallest Aitken size mode is

292   negligible, suggesting that long-range transported (LRT) particles are either dominant over the

293   background marine particle loading or that smaller Aitken mode particles are coagulating onto

294   larger LRT continental aerosols to form a unimodal accumulation mode (Tomlin et al., 2021).
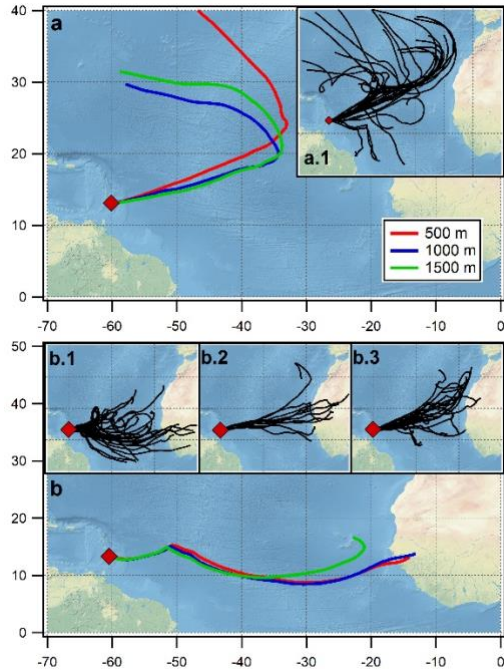
295

296   **Figure 1**: HYSPLIT back trajectories at Ragged Point, Barbados (red diamond) for the

297   EUREC[4]A/ATOMIC field campaign. (a) Back trajectories for 2020/2/8 18:00 UTC at heights of

298   500 m (red), 1000 m (blue), and 1500 m (green) exemplify air mass origins during clean marine

299   sampling conditions. Subplot a.1 shows all back trajectories from clean marine sampling

300   conditions collected at 6 h intervals with a release altitude of 1000 m from 2020/1/29 0:00 –

301   2020/1/29 12:00, 2020/2/6 12:00 – 2020/2/9 18:00 and 2020/2/12 12:00 – 2020/2/15 6:00 UTC.

302   (b) Back trajectories for 2020/2/2 18:00 UTC at 500 m, 1000 m, and 1500 m exemplify air mass

303   origins during CAT conditions. The subplots, b.1, b.2, and b.3 show all back trajectories for 3

304   time periods during which continental aerosols were sampled: b.1) 2020/1/29 18:00 – 2020/2/6

305   6:00, b.2) 2020/2/10 0:00 – 2020/2/12 6:00, and b.3) 2020/2/15 12:00 – 2020/2/20 18:00 UTC.

306   Trajectories for b subplots were also collected at 6 h intervals with a release altitude of 1000 m.

307
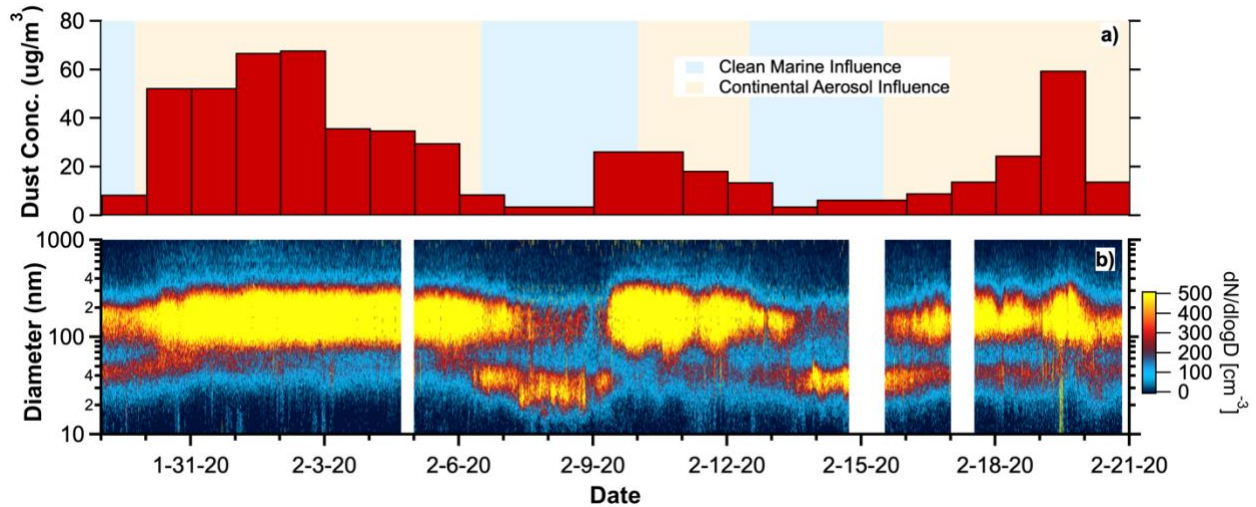
308

309 **Figure 2** – Temporal evolution of (a) dust mass concentrations determined from bulk aerosol

310 filter samples and (b) submicron aerosol particle size distributions determined with an SMPS.

311 Time for both plots is given in UTC (-4 h local Atlantic Standard Time). Color shading in (a)

312 represents continental aerosol influence (orange shading) and clean marine influence (b) as

313 determined by NOAA HYSPLIT back trajectories calculated at Ragged Point.

314

315 Single Particle Aerosol Composition

316 CCSEM/EDX analysis from the EUREC[4]A and ATOMIC campaigns revealed the presence

317 of several particle types with distinct chemistries and morphologies in the submicron aerosol

318 loading (Ault et al., 2014; Behnke et al., 1997; Gaston et al., 2011a, 2013a). Figure 3 presents

319 SEM images (left) and EDX spectra (right) for each particle type detected on stage 3 of the MPS

320 (particle diameter <0.7 µm), including sea spray, aged sea spray, mineral dust, internally mixed

321 mineral dust and sea spray, sulfate, smoke, internally mixed mineral dust and smoke, and

322 organics. Sea spray particles as well as internally mixed mineral dust and sea spray particles

323   were dominant components of the supermicron aerosol loading but are only minor components

324   of submicron aerosol.

325   *Sea Spray*

326   Sea spray particles were characterized by high relative abundance of approximately equal

327   parts Na and Cl, indicating the formation of halite (NaCl). Morphologically, sea spray particles

328   have a cubic shape that represents the crystal structure of halite. Small Mg peaks approximately

329   10% of the height of Na peaks were also observed in NaCl particles and reflect the Na:Mg ratio

330   of seawater. Additional components of sea spray particles include rod-shaped particles

331   containing Ca and S (presumably calcium sulfate) that were often found attached to NaCl

332   particles (Ault et al., 2013; Bondy et al., 2018; Choël et al., 2007). Elements such as N and S that

333   may suggest aging of sea spray were either absent or present in small relative abundance on

334   NaCl components of sea spray particles.

335   *Aged Sea Spray*

336   Aged sea spray was defined by the presence of sea salt components including Na, Mg, K, S,

337   and Cl. In contrast to freshly emitted sea spray particles, aged sea spray has a characteristically

338   low or absent Cl signal with a strong presence of N or S. Figure 3 provides an example of an

339   aged sea spray particle in which Na is high (indicating the presence of salt), but with a low Cl

340   peak (suggesting the particle has been aged). The presence of S in this spectrum may explain the

341   low relative abundance of Cl compared to Na. Sea spray can be aged through reactions with

342   sulfuric acid (H_2SO_4), dinitrogen pentoxide (N_2O_5), and/or nitric acid (HNO_3) which results in Cl

343   depletion and S or N enrichment (Ault et al., 2014; Ault, Guasco, et al., 2013; Behnke et al.,

344   1997; Gaston et al., 2011, 2013; Sobanska et al., 2003). Morphologically, aged sea salt particles

345 had either a similar appearance to fresh sea salt particles, which is often either cubic (as seen in

346 Fig 3), or appeared as a flakey amorphous mass (Hoffman et al., 2004; Laskin et al., 2012; Li et

347 al., 2010).

348 *Mineral Dust*

349   Mineral dust is characterized by the presence of aluminosilicate elements such as Si, Al, Fe,

350 K, Ca, and Mg in EDX spectra, which is consistent with previous studies of African dust

351 (Denjean et al., 2015; Hand et al., 2010; Krueger et al., 2004; Levin et al., 2005; Twohy et al.,

352 2009). Elements such as S and N were not observed in this particle type (Kandler et al., 2018)

353 suggesting that detected dust had not undergone chemical processing during transport. Dust often

354 appeared as a flakey or nodular amorphous mass as exhibited in Fig 3 and previous literature

355 (Krueger et al., 2004; Laskin et al., 2005; Pachauri et al., 2013; Remoundaki et al., 2011).

356 *Internally Mixed Mineral Dust and Sea Spray*

357   Particles containing elements indicative of both mineral dust (Si, Al, Fe, K, Ca, and Mg) and

358 sea salt (approximately equal relative abundances of Na and Cl) were characterized as internally

359 mixed mineral dust and sea spray (Choël et al., 2007; Deboudt et al., 2010; Sobanska et al.,

360 2014). Elements such as S and N were often not present in this particle type, suggesting the

361 particles had not undergone atmospheric aging during transit. Particles containing both dust and

362 sea spray components often appeared as conglomerates of multiple particles with some parts

363 containing more sea spray components and others containing more mineral dust components.

364 *Sulfate*

365   Sulfate-rich particles are a prevalent component of marine submicron aerosol (O'Dowd & de

366 Leeuw, 2007) and characterized here by a dominant S component - often with high relative

367 abundance of C, O, and N. These particles are likely sulfates bound to NH_4^+ such as ammonium

368 sulfate $((NH_4)_2SO_4)$ or ammonium bisulfate (NH_4HSO_4) (Hand et al., 2010). The high relative

369 abundance of C indicates a large organic fraction as well. The morphology of sulfate particles

370 appeared smooth and spherical as reported in previous literature (Nájera & Horn, 2009).

371 *Smoke*

372 Smoke particles were identified by the presence of C with K and S likely representing

373 internally mixed organic and black carbon with potassium-containing salts. K is a well-known

374 indicator for biomass burning (Andreae, 1983; Hand et al., 2010; Hudson et al., 2004; J. Li et al.,

375 2003; Murphy et al., 2006; Pósfai et al., 2003), especially in flaming conditions in Savannah fires

376 as opposed to smoldering conditions (Echalar et al., 1995; Maenhaut et al., 1996).

377 Morphologically, smoke particles can be spherical due to aging or coatings but can also appear

378 as aggregates or chains of spheroids (Dang et al., 2021; Hand et al., 2010; Miller et al., 2021;

379 Pósfai et al., 2003). In this study, smoke particles most frequently appeared as small spherical

380 particles.

381 *Internally Mixed Mineral Dust and Smoke*

382 Internally mixed mineral dust and smoke particles are characterized by dust components such

383 as Si, Al, Fe, Ca, and Mg with strong contributions of K, S, C, and O. Morphologically, internal

384 mixtures of dust and smoke appear as aggregates of amorphous dust particles with clusters or

385 spheres representing soot from smoke. Single particle chemical analysis of these particles show

386 distinctions between the dust and smoke portion of the particle, with the dust portion having

387 typical dust components (Si, Al, Fe, Ca, and Mg) and the smoke portion having typical smoke

388 components (K and S with C and O). Previous research has observed internal mixing of

389 carbonaceous particles and dust particles in Africa when significant amounts of both biomass

390 burning and dust were present (Hand et al., 2010); however, we show that these internal mixtures

391 can be transported all the way to the Caribbean as well.

392 *Organics*

393 Organic particles are defined by strong signals of C and O with few other elements present, if

394 any (Hand et al., 2010). The absence of S or N, which are often indicative of sulfate and nitrate,

395 respectively, suggests that these particles have undergone minimal chemical aging.

396 Morphologically, organic particles are characterized as small individual spheres. The organics

397 were likely marine in origin (Russell et al., 2010) as they were the smallest particle type

398 observed both during clean marine conditions and during CAT conditions, which indicates they

399 may be a "background" aerosol type (Russell et al., 2010).

400
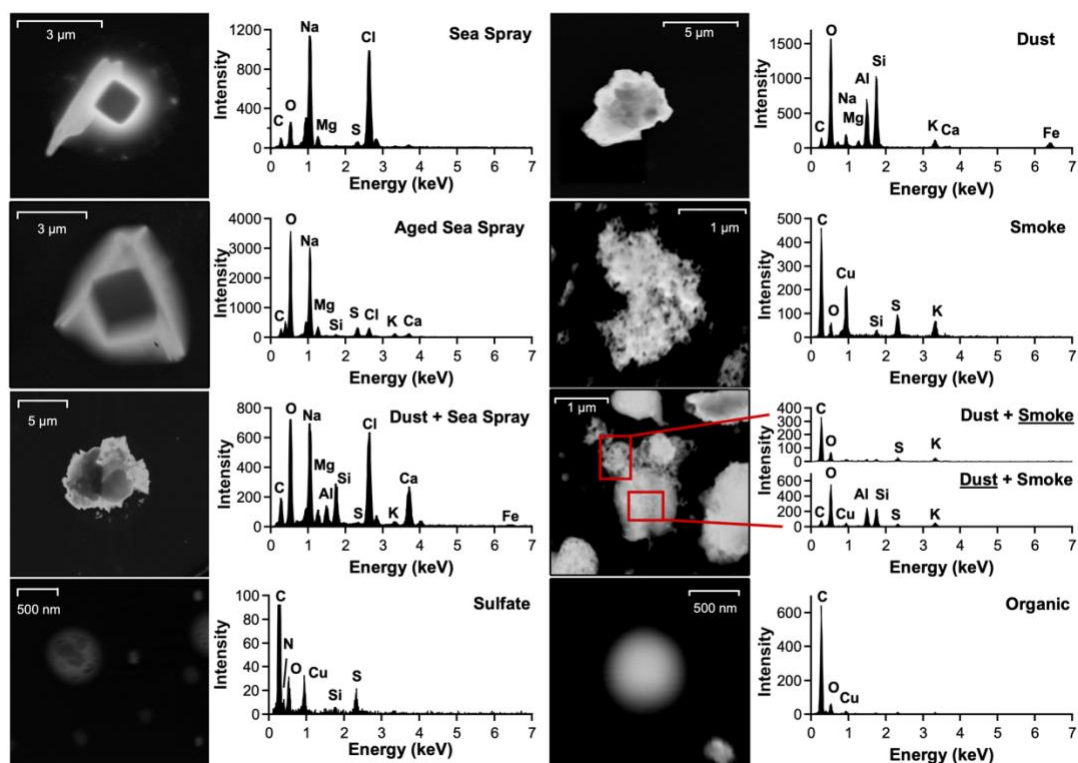
Figure 3: Characteristic aerosol particle types observed by SEM-EDX images (left) and spectra (right) in samples collected during the EUREC^{4}A/ATOMIC campaign. Spectra for the Dust + Smoke particle type represent different areas analyzed on the particle with EDX, denoted by the red boxes.

Arrival of Anomalous Wintertime Co-Transported Dust and Smoke

Figure 4 presents number fractions for particles detected in the submicron aerosol throughout the sampling period and reveals a similar trend in smoke particle number fractions to those of dust mass concentrations in Fig. 2, suggesting that smoke and dust were co-transported to Barbados from Africa. A similar plot to Fig. 4 that contains temporal chemistry from stage 1 and stage 2 of the MPS (representing supermicron particles >0.7 μm diameter) determined using CCSEM/EDX analysis can be found in the SI (Figure S2). During the boreal winter, the Sahel

413   region in North Africa experiences its fire season in which large swathes of land are burned and

414   large plumes of smoke are emitted from the region (Figure S3; Ansmann et al., 2009; Barkley et

415   al., 2019; Roberts et al., 2009). However, due to the southward shift in the ITCZ during boreal

416   winter, smoke is expected to be transported primarily to South America (Moran-Zuloaga et al.,

417   2018; Talbot et al., 1990; Wang et al., 2016). In our study, we observed the arrival of this smoke

418   on Barbados. These findings are supported by temporal carbon monoxide (CO) column density

419   measurements that are often used as a tracer for smoke (Figure S4 and S5). Periods that

420   correspond to clean marine influence are dominated by sulfate and organic particles in the

421   submicron aerosol (Figure 4). Upon arrival of continental aerosols, wildfire smoke appeared to

422   dominate the number fraction of submicron aerosol.
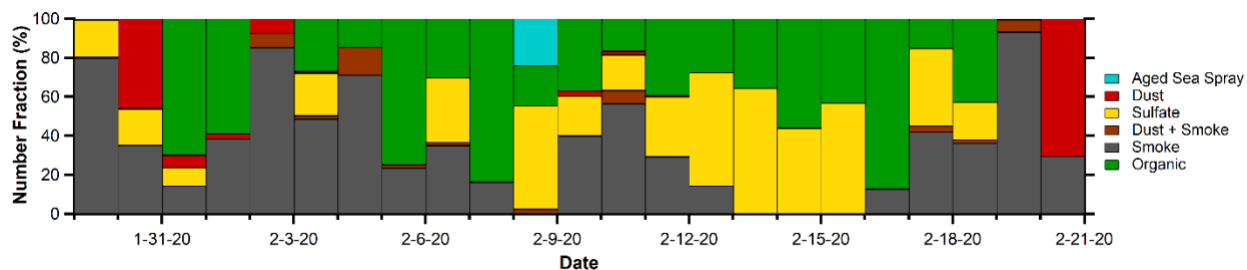
423

424   **Figure 4**: Temporal evolution of submicron number fractions for different types of aerosol

425   particles determined by CCSEM/EDX analysis. The total number of particles analyzed for each

426   day ranges from 1000 to 20,000.

427   Figure 5 presents size-resolved chemical data from CCSEM/EDX analysis from clean

428   marine periods (average of all clean marine periods) and one exemplary time period influenced

429   by continental air masses (CAT event 1). Similar plots for other CAT events are provided in the

430   SI (Figure S6). Average particle diameters for each particle type detected during each sampling

431   period are also provided in Table S1. Figure 5 shows that in clean marine periods, a small

432   fraction of large particles have both a smoke and a dust signature. This suggests that our "clean

433   marine conditions" are only "clean" relative to time periods dominated by dust and smoke, rather

434   than pristine clean marine conditions without any continental aerosol influence. The CAT event

435   plot in Fig. 5 demonstrates that dust as well as internally mixed dust and smoke particles

436   dominate in the submicron aerosol loading, followed by smoke. Smoke particles follow as the

437   next largest particle type. Organics dominate in the smallest size fractions, followed by sulfates,

438   suggesting a secondary source for sulfate (Bates et al., 1992). Aged sea salt particles were on

439   average smaller than most dust, internally mixed dust and smoke, and smoke particles. Figure 5

440   also shows that at a diameter of ~0.1µm (which is approximately the d_{50} of CCN at S 0.16% in

441   clean marine conditions and CAT conditions) the composition is dominated by sulfates and

442   organics in the clean marine conditions, while smoke and organics dominate in the CAT event.

443   The large decrease in sulfate number fraction during CAT events might be caused by the

444   condensation of Aitken mode sulfate-containing particles onto larger, long-range transported

445   particles as indicated in Fig. 2 (Gaston et al., 2010).

446
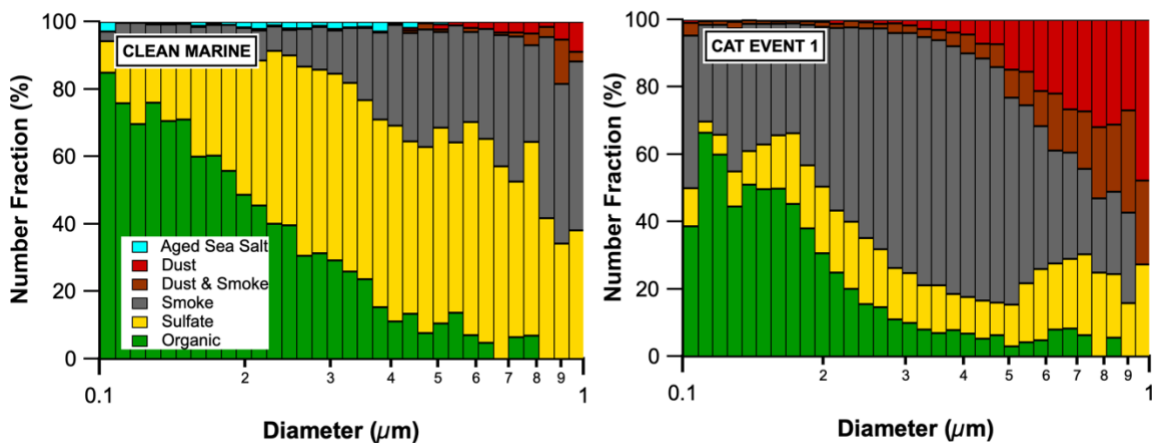
447

448   **Figure 5:** Number fractions of different types of submicron aerosol particles plotted against

449   particle diameter. The "clean marine" plot (left) includes data from all clean marine sampling

450   periods. The "CAT Event 1" plot (right) includes data from the first period in which dust and

451   wildfire smoke were observed over Barbados (2020/1/29 18:00 – 2020/2/6 6:00 UTC). Particles

452   were organized into 32 size cuts (bins) to maximize resolution of size-resolved chemical data.

453   Particle counts in each bin range from 34 particles to up to 3041 with an average bin count of

454   493 particles for the Clean Marine plot and 973 for the CAT Event plot.

455

456   Changes in Aerosol Hygroscopicity during EUREC⁴A/ATOMIC

457   Comparisons between κ and submicron single particle elemental composition reveal that

458   smoke particles lower the hygroscopicity of the submicron aerosol compared to marine-derived

459   submicron aerosol in the tropical North Atlantic. Figure 6 presents boxplots for κ values as well

460   as average d_{50} measured at each S during both clean marine conditions and CAT conditions.

461   Both plots show a similar trend in which average κ increases from 0.09% S to 0.24% S. Then,

462   with each subsequent increase in S after 0.24% S, κ decreases as smaller, less hygroscopic

463   particles activate at higher supersaturations. The low hygroscopicity of these smaller particles

464   can be explained by compositional changes in the aerosol loading exhibited in Fig 5, reflecting

465   the shift in particle chemistry from mostly sulfate to mostly organic with decreasing particle size.

466   Also of note is the κ of 0.6 observed for clean marine conditions at 0.24% S, which matches κ

467   measurements for ammonium sulfate particles that can dominate along with sea spray organics

468   during clean marine conditions (Petters & Kreidenweis, 2007).

469   There is also a noticeable drop in average κ between the same supersaturations in clean

470   marine conditions compared to CAT conditions. For example, at 0.16% S, $\kappa=0.52\pm0.09$ for all

471   clean marine condition periods and $\kappa=0.46\pm0.10$ for all continental aerosol transport periods.

472 This is likely due to the addition of less hygroscopic material such as dust and smoke particles

473 that are not dominant in clean marine conditions. As expected, trends in average d_{50} for both

474 plots indicate that smaller particles activate as CCN with larger supersaturations. Activation

475 diameters during CAT conditions are also larger than corresponding activation diameters in clean

476 marine conditions for the same supersaturation. This also suggests that the addition of less

477 soluble material from transported smoke particles lowers the hygroscopicity and increases the

478 activation diameter.

479   When comparing hygroscopicity data from this study to previous research, we find both

480 similarities and differences in κ trends. For example, Good et al. (2010) presents data collected in

481 the tropical eastern Atlantic that provides an ideal comparison to our findings. On average, their

482 values for κ in clean marine conditions and during observations of dust transport (κ=1.15-1.4 and

483 0.8-0.92, respectively) were much higher than our observed values. However, Good et al. (2010)

484 shows similarities to our work through the distinct drop in κ between clean marine conditions

485 and CAT conditions which is attributed to the addition of hydrophobic dust to the aerosol

486 loading. Wex et al. (2016) present CCN data from ground-based field sampling in November and

487 April at Ragged Point, Barbados. They show a similar trend in κ in which values increase from

488 0.1% S, peak at 0.2% S, then decrease with each subsequent increase in S. They also found a

489 similar drop in κ upon the arrival of long-range transported aerosols, likely due to less

490 hygroscopic particles from continental sources activating as CCN. A separate study from

491 Kristensen et al. (2016) conducted similar research at Ragged Point, Barbados during the boreal

492 summer. The range in κ values of 0.2-0.5 match those observed in our work, especially during

493 CAT events. However, Kristensen et al. (2016) determined that concentrations of dust, sea salt,

494 and soot were too small to influence CCN, concluding that sulfates and organics were the

495   primary CCN types. They conclude that the low κ values observed during their sampling were

496   due to organic compounds activating as CCN. We find similar κ values to Kristensen et al.

497   (2016) and a similar particle chemistry of the accumulation and Aikten modes during clean

498   marine conditions, suggesting that organics and sulfates were the primary CCN types during

499   clean marine conditions studied for the EUREC[4]A and ATOMIC campaigns as well. We also

500   observe a drop κ from clean marine conditions to CAT events. This drop in κ indicates the

501   influence of an additional CCN particle type contributed by the CAT events.
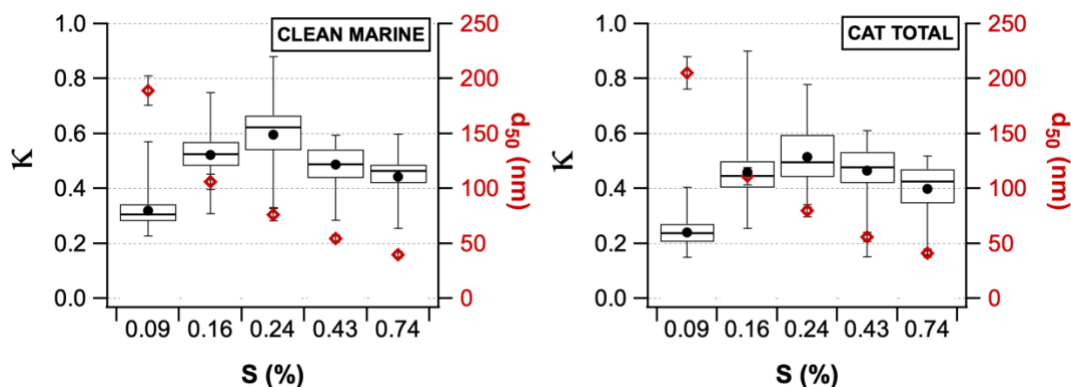
502

503   **Figure 6:** Hygroscopicity parameter κ (left axis, box plots) and corresponding mean

504   diameter at which 50% of the particles in an aerosol population activate as CCN at a particular S,

505   also called the critical diameter "d_{50}" (right axis; red markers) for the investigated

506   supersaturations (S). Whiskers on "d_{50}" markers represent standard deviation values of "d_{50}".

507   Black dots in the boxplot indicate κ mean values. Boxes represent the upper quartile, median,

508   and lower quartile κ values at each S. Whiskers represent the upper and lower limit of κ at each

509   S.

510

511

512   African Smoke Particles Enhance CCN Concentrations

513   Comparisons between smoke fractions and CCN counts suggest that smoke particles

514 enhance the number of CCN in the tropical North Atlantic MBL. Figure 7 presents two temporal

515 plots of κ (Figure 7a) and smoke number fractions with CCN counts measured at 0.16% S

516 (Figure 7b). Table 1 provides averages of CCN concentrations for each time period shown in

517 Fig. 7b. Table S2 also provides average and median counts of analyzed smoke particles

518 calculated for each CAT event, including CAT Event 3 which had fewer smoke particles and a

519 higher κ compared to other CAT Events. Figure 7 suggests that there is an inverse relationship

520 between κ and smoke number fractions in which an increase in smoke particles results in a

521 decrease in κ. This is likely due to the activation of smoke particles as CCN, which are on

522 average less hygroscopic than the sulfate particles that act as CCN during clean marine

523 conditions. Figure 7b shows a positive correlation between smoke number fractions and CCN

524 counts. A correlation plot of smoke number fraction and CCN concentrations is also provided in

525 Fig. S7 to further emphasize their direct relationship.

526   There are multiple possible explanations for why African smoke particles may have acted

527 as CCN. As shown in Fig. 5, smoke particles are larger than organics and sulfates, on average,

528 and dominate sulfate and organic particle number concentrations upon arrival of long-range

529 transported African aerosols. In this case, the relatively large size of the smoke particles makes

530 for better CCN compared to organics or sulfates via the Kelvin effect (Dusek et al., 2006). The

531 presence of salts in smoke particles has also been shown to be an important component in smoke

532 hygroscopicity and may explain why smoke is efficient as CCN. Previous studies have shown

533 that smoke particles often contain hygroscopic salts such as potassium chloride, potassium

534 sulfate, and potassium nitrate (e.g., KCl, KNO_3, and K_2SO_4) (Dang et al., 2022; Freney et al.,

535 2009; Zauscher et al., 2013). Other research also shows that only small fractions of salts are

536 needed to increase aerosol hygroscopicity (Roberts et al., 2002). Based on CCSEM/EDX

537 analysis, we find evidence that potassium sulfate salts may be present in transported smoke

538 particles, and thus may explain the potential for smoke to act as CCN.
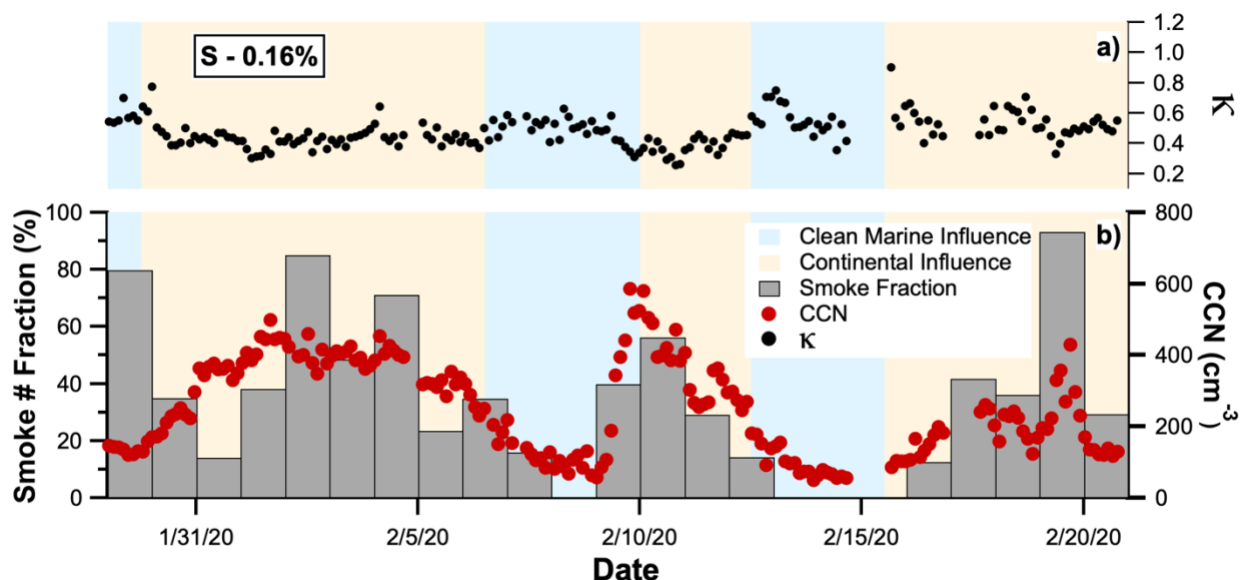
540 **Figure 7**: Temporal evolution of hygroscopicity parameter κ (black dots, upper panel) and CCN

541 number concentration (red dots, lower panel), both measured at S = 0.16%, and smoke particle

542 number fraction (grey bars, left axis, lower panel). Background color shadings indicate periods

543 of continental influence (orange) and clean marine influence (blue) determined by HYSPLIT

544 back trajectories and dust mass concentrations.

545 **Table 1** – Values for average CCN Concentrations and κ measured at 0.16% S during each clean

546 marine influence period and CAT event sampled during the EUREC[4]A and ATOMIC

547 campaigns.

Sampling Period	Day/Time	CCN Concentrations (pt/cm^3)	Average κ
Clean Marine Period 1	2020/1/29 0:00 – 2020/1/29 12:00	140±10	0.58±0.07
CAT Event 1	2020/1/29 18:00 – 2020/2/6 6:00	340±90	0.44±0.08
Clean Marine Period 2	2020/2/6 12:00 – 2020/2/9 18:00	150±98	0.50±0.10

CAT Event 2	2020/2/10 0:00 – 2020/2/12 6:00	400 ± 106	0.38 ± 0.06
Clean Marine Period 3	2020/2/12 12:00 – 2020/2/15 6:00	100 ± 42	0.55 ± 0.10
CAT Event 3	2020/2/15 12:00 – 2020/2/20 – 18:00	190 ± 75	0.54 ± 0.10

548

Conclusions

550   During clean marine conditions, the submicron aerosol loading consists primarily of

551 sulfate and organic particles. CCN measurements determine cloud activation by particles

552 approximately 80 nm in activation diameter with an average $\kappa = 0.52\pm0.08$ for 0.16% S.

553 Comparisons between particle size, hygroscopicity, and single particle elemental composition

554 suggest that sulfate particles (likely ammonium sulfate) are the primary CCN particles in clean

555 marine conditions. During the EUREC[4]A/ATOMIC campaign, Barbados received three African

556 aerosol transport events during which we detected mineral dust and smoke particles from

557 northern Africa. Upon the arrival of African aerosols to BACO, CCN average activation

558 diameter increased to approximately 200 nm while the average hygroscopicity of activated

559 particles for all CAT events decreased to $\kappa = 0.45\pm0.1$ for 0.16% S. Upon arrival of high

560 concentrations of smoke particles to Barbados, smoke particles dominate the accumulation mode

561 particle loading, decrease aerosol hygroscopicity, and also increase CCN number concentrations,

562 which could also increase the cloud droplet number concentration and alter cloud radiative

563 properties (Twomey, 1974). Overall, we find that smoke has a large effect on CCN number

564 concentrations during the boreal winter when smoke transport is high.

565   The observation of smoke transported to Barbados during the boreal winter also indicates

566 the large geographic extent of African smoke that can impact the MBL. Building upon recent

567 work from Ragged Point and other parts of the tropical and subtropical Atlantic (Holanda et al.,

568 2020; Kacarab et al., 2020; Schill et al., 2020; Zuidema et al., 2018) this work also indicates a

569   need for greater consideration of the impacts of smoke in the MBL, especially during the boreal

570   winter. Previous research conducted at Ragged Point has primarily focused on African dust,

571   which reaches its maximum during the boreal summer when smoke transport is low (Zuidema et

572   al., 2019). To better contextualize our findings, we analysed carbon monoxide column density (a

573   tracer for smoke) as well as aerosol optical depth (AOD; a tracer for dust and smoke) from 2018-

574   2022 (Figure S4 and S5). Figure S4 shows the temporal trends while Fig. S5 show seasonal

575   averages. As expected, AOD peaks in July when dust transport reaches a maximum. However,

576   Fig. S4 and S5 indicate that smoke is decoupled from dust, reaching a maximum in the spring

577   around April and a minimum in the summer when dust transport is highest. This finding suggests

578   that while the dust transport during the EUREC4A/ATOMIC campaigns is higher than average

579   dust loadings during this month (Zuidema et al., 2019), the amount of smoke observed is not

580   unique, but rather characteristic of the region. This is consistent with observations in Amazonia,

581   where smoke and dust transport during boreal winter and spring has been found consistently

582   since the first measurement campaign in 1987 (Talbot et al., 1990; Andreae et al., 2015; Moran-

583   Zuloaga et al., 2018) . Further, wintertime aerosol transport is typically transported at lower

584   altitudes as the height of emission for wintertime aerosols is lower compared to summertime

585   aerosol transport, leading to greater mixing into the MBL (Gutleben et al., 2022; Tsamalis et al.,

586   2013). Thus, smoke may be playing an important role on CCN formation throughout a large

587   portion of the year. This is especially true considering the large size of long-range transported

588   smoke plumes that have a wide geographic extent in which they can affect cloud formation. To

589   conclude, this work highlights the need to characterize African smoke transport to Ragged Point

590   and better understand the role of smoke in cloud formation, radiative forcing, and climate

591   (Pechony & Shindell, 2010; Shindell et al., 2009).

Data Availability

The data will be made publically available in the University of Miami data repository and will be linked with a doi.

Author Contributions

Conceptualization of this work was done by HMR, MLP, OK, and CJG. Collection of samples was conducted by HMR, OK, EB, and PS, while analysis was done by HMR, MLP, OK, NNL, and ZC. The development of the methods used in this work was done by HMR, MLP, OK, ZC, SC, APA, and CJG. Instrumentation used to conduct this work were provided by MLP, SC, APA, and CJG. Formal analysis of data was performed by HMR, MLP, CP, and OK. Validation of data products was performed by HMR, ZC, SC, APA, and CJG. Computer code used for data analysis was provided by MLP, OK, and APA. Data visualization was performed by HMR, MLP, and OK. PKQ, PZ, CP, and UP helped interpret results. Supervision and project administration duties were done by MLP and CJG. HMR wrote the original draft for publication, and all co-authors reviewed and edited this work.

Competing Interests

Some authors are members of the editorial board of Atmospheric Chemistry and Physics. The peer-review process was guided by an independent editor, and the authors have no other competing interests to declare

Acknowledgements

C.J.G. acknowledges an NSF CAREER award (1944958). A portion of this research was performed on project awards (10.46936/lser.proj.2019.50816/60000110 and 10.46936/lser.proj.2021.51900/60000361) from the Environmental Molecular Sciences Laboratory, a DOE Office of Science User Facility sponsored by the Biological and Environmental Research program under Contract No. DE-AC05-76RL01830. P.K.Q. acknowledges PMEL contribution number 5353. MLP and CP acknowledge support by the Max Planck Society. P.Z. acknowledges support from the NOAA grant OAR CPO NA19OAR4310379.

625

626

627

628   References

629   Abel, S. J., Haywood, J. M., Highwood, E. J., Li, J., & Buseck, P. R. (2003). Evolution of biomass
630   burning aerosol properties from an agricultural fire in southern Africa. *Geophysical Research*
631   *Letters*, *30*(15). https://doi.org/https://doi.org/10.1029/2003GL017342

632   Adams, A. M., Prospero, J. M., & Zhang, C. (2012). CALIPSO-Derived Three-Dimensional Structure of
633   Aerosol over the Atlantic Basin and Adjacent Continents. *Journal of Climate*, *25*, 6862–6879.

634   Albrecht, B. A. (1989). Aerosols, cloud microphysics, and fractional cloudiness. *Science*, *245*(4923),
635   1227–1230. https://doi.org/10.1126/science.245.4923.1227

636   Allan, J. D., Baumgardner, D., Raga, G. B., Mayol-Bracero, O. L., Morales-García, F., García-García, F.,
637   Montero-Martínez, G., Borrmann, S., Schneider, J., Mertes, S., Walter, S., Gysel, M., Dusek, U.,
638   Frank, G. P., & Krämer, M. (2008). Clouds and aerosols in Puerto Rico – a new evaluation.
639   *Atmospheric Chemistry and Physics*, *8*(5), 1293–1309. https://doi.org/10.5194/acp-8-1293-2008

640   Andreae, M. O. (1983). Soot Carbon and Excess Fine Potassium: Long-Range Transport of Combustion-
641   Derived Aerosols. *Science*, *220*(4602), 1148–1151. https://doi.org/10.1126/science.220.4602.1148

642   Andreae, M. O. (2019). Emission of trace gases and aerosols from biomass burning -- an updated
643   assessment. *Atmospheric Chemistry and Physics*, *19*(13), 8523–8546. https://doi.org/10.5194/acp-
644   19-8523-2019

645   Ansmann, A., Baars, H., Tesche, M., Müller, D., Althausen, D., Engelmann, R., Pauliquevis, T., &
646   Artaxo, P. (2009). Dust and smoke transport from Africa to South America: Lidar profiling over
647   Cape Verde and the Amazon rainforest. *Geophysical Research Letters*, *36*(11).
648   https://doi.org/https://doi.org/10.1029/2009GL037923

649   Archibald, A. T., Witham, C. S., Ashfold, M. J., Manning, A. J., O'Doherty, S., Greally, B. R., Young,
650   D., & Shallcross, D. E. (2015). Long-term high frequency measurements of ethane, benzene and
651   methyl chloride at Ragged Point, Barbados: Identification of long-range transport events. *Elementa:*
652   *Science of the Anthropocene*, *3*. https://doi.org/10.12952/journal.elementa.000068

653   Ault, A. P., Guasco, T. L., Baltrusaitis, J., Ryder, O. S., Trueblood, J. v, Collins, D. B., Ruppel, M. J.,
654   Cuadra-Rodriguez, L. A., Prather, K. A., & Grassian, V. H. (2014). Heterogeneous Reactivity of
655   Nitric Acid with Nascent Sea Spray Aerosol: Large Differences Observed between and within
656   Individual Particles. *The Journal of Physical Chemistry Letters*, *5*(15), 2493–2500.
657   https://doi.org/10.1021/jz5008802

658   Ault, A. P., Guasco, T. L., Ryder, O. S., Baltrusaitis, J., Cuadra-Rodriguez, L. A., Collins, D. B., Ruppel,
659   M. J., Bertram, T. H., Prather, K. A., & Grassian, V. H. (2013). Inside versus outside: Ion

redistribution in nitric acid reacted sea spray aerosol particles as determined by single particle analysis. *Journal of the American Chemical Society*, *135*(39), 14528–14531. https://doi.org/10.1021/ja407117x

Ault, A. P., Moffet, R. C., Baltrusaitis, J., Collins, D. B., Ruppel, M. J., Cuadra-Rodriguez, L. A., Zhao, D., Guasco, T. L., Ebben, C. J., Geiger, F. M., Bertram, T. H., Prather, K. A., & Grassian, V. H. (2013). Size-Dependent Changes in Sea Spray Aerosol Composition and Properties with Different Seawater Conditions. *Environmental Science & Technology*, *47*(11), 5603–5612. https://doi.org/10.1021/es400416g

Ault, A. P., Peters, T. M., Sawvel, E. J., Casuccio, G. S., Willis, R. D., Norris, G. A., & Grassian, V. H. (2012). Single-Particle SEM-EDX Analysis of Iron-Containing Coarse Particulate Matter in an Urban Environment: Sources and Distribution of Iron within Cleveland, Ohio. *Environmental Science & Technology*, *46*(8), 4331–4339. https://doi.org/10.1021/es204006k

Ault, A. P., Zhao, D., Ebben, C. J., Tauber, M. J., Geiger, F. M., Prather, K. A., & Grassian, V. H. (2013). Raman microspectroscopy and vibrational sum frequency generation spectroscopy as probes of the bulk and surface compositions of size-resolved sea spray aerosol particles. *Physical Chemistry Chemical Physics*, *15*(17), 6206–6214. https://doi.org/10.1039/C3CP43899F

Barkley, A. E., Olson, N. E., Prospero, J. M., Gatineau, A., Panechou, K., Maynard, N. G., Blackwelder, P., China, S., Ault, A. P., & Gaston, C. J. (2021). Atmospheric Transport of North African Dust-Bearing Supermicron Freshwater Diatoms to South America: Implications for Iron Transport to the Equatorial North Atlantic Ocean. *Geophysical Research Letters*, *48*(5), e2020GL090476. https://doi.org/https://doi.org/10.1029/2020GL090476

Barkley, A. E., Prospero, J. M., Mahowald, N., Hamilton, D. S., Popendorf, K. J., Oehlert, A. M., Pourmand, A., Gatineau, A., Panechou-Pulcherie, K., Blackwelder, P., & Gaston, C. J. (2019). African biomass burning is a substantial source of phosphorus deposition to the Amazon, Tropical Atlantic Ocean, and Southern Ocean. *Proceedings of the National Academy of Sciences*, *116*(33), 16216 LP – 16221. https://doi.org/10.1073/pnas.1906091116

Bates, T. S., Lamb, B. K., Guenther, A., Dignon, J., & Stoiber, R. E. (1992). Sulfur emissions to the atmosphere from natural sourees. *Journal of Atmospheric Chemistry*, *14*(1), 315–337. https://doi.org/10.1007/BF00115242

Behnke, W., George, C., Scheer, V., & Zetzsch, C. (1997). Production and decay of ClNO2 from the reaction of gaseous N2O5 with NaCl solution: Bulk and aerosol experiments. *Journal of Geophysical Research Atmospheres*, *102*(3), 3795–3804. https://doi.org/10.1029/96jd03057

Behrenfeld, M. J., Moore, R. H., Hostetler, C. A., Graff, J., Gaube, P., Russell, L. M., Chen, G., Doney, S. C., Giovannoni, S., Liu, H., Proctor, C., Bolaños, L. M., Baetge, N., Davie-Martin, C., Westberry, T. K., Bates, T. S., Bell, T. G., Bidle, K. D., Boss, E. S., … Ziemba, L. (2019). The North Atlantic Aerosol and Marine Ecosystem Study (NAAMES): Science Motive and Mission Overview . In *Frontiers in Marine Science* (Vol. 6). https://www.frontiersin.org/article/10.3389/fmars.2019.00122

Bondy, A. L., Bonanno, D., Moffet, R. C., Wang, B., Laskin, A., & Ault, A. P. (2018). The diverse chemical mixing state of aerosol particles in the southeastern United States. *Atmospheric Chemistry and Physics*, *18*(16), 12595–12612. https://doi.org/10.5194/acp-18-12595-2018

Capes, G., Johnson, B., McFiggans, G., Williams, P. ~I., Haywood, J., & Coe, H. (2008). Aging of biomass burning aerosols over West Africa: Aircraft measurements of chemical composition, microphysical properties, and emission ratios. *Journal of Geophysical Research (Atmospheres)*, *113*(D23), D00C15. https://doi.org/10.1029/2008JD009845

Cappa, C. D., Lim, C. Y., Hagan, D. H., Coggon, M., Koss, A., Sekimoto, K., de Gouw, J., Onasch, T. B., Warneke, C., & Kroll, J. H. (2020). Biomass-burning-derived particles from a wide variety of fuels - - Part 2: Effects of photochemical aging on particle optical and chemical properties. *Atmospheric Chemistry and Physics*, *20*(14), 8511–8532. https://doi.org/10.5194/acp-20-8511-2020

Carlson, T. N., & Prospero, J. M. (1972). The Large-Scale Movement of Saharan Air Outbreaks over the Northern Equatorial Atlantic. *Journal of Applied Meteorology and Climatology*, *11*(2), 283–297. https://doi.org/10.1175/1520-0450(1972)011<0283:TLSMOS>2.0.CO;2

Carslaw, K. S., Lee, L. A., Reddington, C. L., Pringle, K. J., Rap, A., Forster, P. M., Mann, G. W., Spracklen, D. v, Woodhouse, M. T., Regayre, L. A., & Pierce, J. R. (2013). Large contribution of natural aerosols to uncertainty in indirect forcing. *Nature*, *503*(7474), 67–71. https://doi.org/10.1038/nature12674

Chin, M., Diehl, T., Tan, Q., Prospero, J. M., Kahn, R. A., Remer, L. A., Yu, H., Sayer, A. M., Bian, H., Geogdzhayev, I. v, Holben, B. N., Howell, S. G., Huebert, B. J., Hsu, N. C., Kim, D., Kucsera, T. L., Levy, R. C., Mishchenko, M. I., Pan, X., … Zhao, X.-P. (2014). Multi-decadal aerosol variations from 1980 to 2009: a perspective from observations and a global model. *Atmospheric Chemistry and Physics*, *14*(7), 3657–3690. https://doi.org/10.5194/acp-14-3657-2014

Choël, M., Deboudt, K., Flament, P., Aimoz, L., & Mériaux, X. (2007). Single-particle analysis of atmospheric aerosols at Cape Gris-Nez, English Channel: Influence of steel works on iron apportionment. *Atmospheric Environment*, *41*(13), 2820–2830. https://doi.org/https://doi.org/10.1016/j.atmosenv.2006.11.038

Dang, C., Segal-Rozenhaimer, M., Che, H., Zhang, L., Formenti, P., Taylor, J., Dobracki, A., Purdue, S., Wong, P.-S., Nenes, A., Sedlacek, A., Coe, H., Redemann, J., Zuidema, P., & Haywood, J. (2021). Biomass burning and marine aerosol processing over the southeast Atlantic Ocean: A TEM single particle analysis. *Atmos. Chem. Phys. Discuss.*, *2021*, 1–30. https://doi.org/10.5194/acp-2021-724

Dang, C., Segal-Rozenhaimer, M., Che, H., Zhang, L., Formenti, P., Taylor, J., Dobracki, A., Purdue, S., Wong, P.-S., Nenes, A., Sedlacek III, A., Coe, H., Redemann, J., Zuidema, P., Howell, S., & Haywood, J. (2022). Biomass burning and marine aerosol processing over the southeast Atlantic Ocean: a TEM single-particle analysis. *Atmospheric Chemistry and Physics*, *22*(14), 9389–9412. https://doi.org/10.5194/acp-22-9389-2022

Deboudt, K., Flament, P., Choël, M., Gloter, A., Sobanska, S., & Colliex, C. (2010). Mixing state of aerosols and direct observation of carbonaceous and marine coatings on African dust by individual particle analysis. *Journal of Geophysical Research: Atmospheres*, *115*(D24). https://doi.org/https://doi.org/10.1029/2010JD013921

Denjean, C., Caquineau, S., Desboeufs, K., Laurent, B., Maille, M., Quiñones Rosado, M., Vallejo, P., Mayol-Bracero, O. L., & Formenti, P. (2015). Long-range transport across the Atlantic in summertime does not enhance the hygroscopicity of African mineral dust. *Geophysical Research Letters*, *42*(18), 7835–7843. https://doi.org/https://doi.org/10.1002/2015GL065693

741 Dusek, U., Frank, G. P., Hildebrandt, L., Curtius, J., Schneider, J., Walter, S., Chand, D., Drewnick, F.,
742   Hings, S., Jung, D., Borrmann, S., & Andreae, M. O. (2006). Size Matters More Than Chemistry for
743   Cloud-Nucleating Ability of Aerosol Particles. *Science*, *312*(5778), 1375–1378.
744   https://doi.org/10.1126/science.1125261

745 Echalar, F., Gaudichet, A., Cachier, H., & Artaxo, P. (1995). Aerosol emissions by tropical forest and
746   savanna biomass burning: Characteristic trace elements and fluxes. *Geophysical Research Letters*,
747   *22*(22), 3039–3042. https://doi.org/https://doi.org/10.1029/95GL03170

748 Edwards, E.-L., Corral, A. F., Dadashazar, H., Barkley, A. E., Gaston, C. J., Zuidema, P., & Sorooshian,
749   A. (2021). Impact of various air mass types on cloud condensation nuclei concentrations along
750   coastal southeast Florida. *Atmospheric Environment*, *254*, 118371.
751   https://doi.org/https://doi.org/10.1016/j.atmosenv.2021.118371

752 Forster, P., Storelvmo, T., Armour, K., William, C., Dufresne, J.-L., Frame, D., Lunt, D., Mauritsen, T.,
753   Palmer, M., Watanabe, M., Wild, M., & Zhang, H. (2021). Chapter 7: The Earth's energy budget,
754   climate feedbacks, and climate sensitivity. *Climate Change 2021: The Physical Science Basis*,
755   *Contributi*.

756 Freney, E. J., Martin, S. T., & Buseck, P. R. (2009). Deliquescence and efflorescence of potassium salts
757   relevant to biomass-burning aerosol particles. *Aerosol Science and Technology*, *43*(8), 799–807.
758   https://doi.org/10.1080/02786820902946620

759 Gaston, C. J., Furutani, H., Guazzotti, S. A., Coffee, K. R., Bates, T. S., Quinn, P. K., Aluwihare, L. I.,
760   Mitchell, B. G., & Prather, K. A. (2011). Unique ocean-derived particles serve as a proxy for
761   changes in ocean chemistry. *Journal of Geophysical Research Atmospheres*, *116*(18), 1–13.
762   https://doi.org/10.1029/2010JD015289

763 Gaston, C. J., Pratt, K. A., Qin, X., & Prather, K. A. (2010). Real-time detection and mixing state of
764   methanesulfonate in single particles at an inland urban location during a phytoplankton bloom.
765   *Environmental Science and Technology*, *44*(5), 1566–1572. https://doi.org/10.1021/es902069d

766 Gaston, C. J., Quinn, P. K., Bates, T. S., Gilman, J. B., Bon, D. M., Kuster, W. C., & Prather, K. A.
767   (2013). The impact of shipping, agricultural, and urban emissions on single particle chemistry
768   observed aboard the R/V Atlantis during CalNex. *Journal of Geophysical Research Atmospheres*,
769   *118*(10), 5003–5017. https://doi.org/10.1002/jgrd.50427

770 Giordano, M., Espinoza, C., & Asa-Awuku, A. (2015). Experimentally measured morphology of biomass
771   burning aerosol and its impacts on CCN ability. *Atmospheric Chemistry and Physics*, *15*(4), 1807–
772   1821. https://doi.org/10.5194/acp-15-1807-2015

773 Good, N., Topping, D. O., Allan, J. D., Flynn, M., Fuentes, E., Irwin, M., Williams, P. I., Coe, H., &
774   McFiggans, G. (2010). Consistency between parameterisations of aerosol hygroscopicity and CCN
775   activity during the RHaMBLe discovery cruise. *Atmos. Chem. Phys.*, *10*(7), 3189–3203.
776   https://doi.org/10.5194/acp-10-3189-2010

777 Gutleben, M., Groß, S., Heske, C., & Wirth, M. (2022). Wintertime Saharan dust transport towards the
778   Caribbean: an airborne lidar case study during EUREC^{4}A. *Atmospheric Chemistry and Physics*,
779   *22*(11), 7319–7330. https://doi.org/10.5194/acp-22-7319-2022

780 Hand, V. L., Capes, G., Vaughan, D. J., Formenti, P., Haywood, J. M., & Coe, H. (2010). Evidence of
781   internal mixing of African dust and biomass burning particles by individual particle analysis using

electron beam techniques. *Journal of Geophysical Research: Atmospheres*, *115*(D13).
https://doi.org/https://doi.org/10.1029/2009JD012938

Hennigan, C. J., Miracolo, M. A., Engelhart, G. J., May, A. A., Presto, A. A., Lee, T., Sullivan, A. P.,
McMeeking, G. R., Coe, H., Wold, C. E., Hao, W.-M., Gilman, J. B., Kuster, W. C., de Gouw, J.,
Schichtel, B. A., Collett Jr., J. L., Kreidenweis, S. M., & Robinson, A. L. (2011). Chemical and
physical transformations of organic aerosol from the photo-oxidation of open biomass burning
emissions in an environmental chamber. *Atmospheric Chemistry and Physics*, *11*(15), 7669–7686.
https://doi.org/10.5194/acp-11-7669-2011

Hennigan, C. J., Sullivan, A. P., Collett Jr., J. L., & Robinson, A. L. (2010). Levoglucosan stability in
biomass burning particles exposed to hydroxyl radicals. *Geophysical Research Letters*, *37*(9).
https://doi.org/https://doi.org/10.1029/2010GL043088

Hodshire, A. L., Akherati, A., Alvarado, M. J., Brown-Steiner, B., Jathar, S. H., Jimenez, J. L.,
Kreidenweis, S. M., Lonsdale, C. R., Onasch, T. B., Ortega, A. M., & Pierce, J. R. (2019). Aging
Effects on Biomass Burning Aerosol Mass and Composition: A Critical Review of Field and
Laboratory Studies. *Environmental Science & Technology*, *53*(17), 10007–10022.
https://doi.org/10.1021/acs.est.9b02588

Hoffman, R. C., Laskin, A., & Finlayson-Pitts, B. J. (2004). Sodium nitrate particles: physical and
chemical properties during hydration and dehydration, and implications for aged sea salt aerosols.
Journal of Aerosol Science, *35*(7), 869–887.
https://doi.org/https://doi.org/10.1016/j.jaerosci.2004.02.003

Holanda, B. A., Pöhlker, M. L., Walter, D., Saturno, J., Sörgel, M., Ditas, J., Ditas, F., Schulz, C., Franco,
M. A., Wang, Q., Donth, T., Artaxo, P., Barbosa, H. M. J., Borrmann, S., Braga, R., Brito, J.,
Cheng, Y., Dollner, M., Kaiser, J. W., … Pöhlker, C. (2020). Influx of African biomass burning
aerosol during the Amazonian dry season through layered transatlantic transport of black carbon-
rich smoke. *Atmospheric Chemistry and Physics*, *20*(8), 4757–4785. https://doi.org/10.5194/acp-20-
4757-2020

Hoppel, W. A., Frick, G. M., & Larson, R. E. (1986). Effect of nonprecipitating clouds on the aerosol size
distribution in the marine boundary layer. *Geophysical Research Letters*, *13*(2), 125–128.
https://doi.org/https://doi.org/10.1029/GL013i002p00125

Hudson, P. K., Murphy, D. M., Cziczo, D. J., Thomson, D. S., de Gouw, J. A., Warneke, C., Holloway, J.,
Jost, H.-J., & Hübler, G. (2004). Biomass-burning particle measurements: Characteristic
composition and chemical processing. *Journal of Geophysical Research: Atmospheres*, *109*(D23).
https://doi.org/https://doi.org/10.1029/2003JD004398

Kacarab, M., Thornhill, K. L., Dobracki, A., Howell, S. G., O'Brien, J. R., Freitag, S., Poellot, M. R.,
Wood, R., Zuidema, P., Redemann, J., & Nenes, A. (2020). Biomass burning aerosol as a modulator
of the droplet number in the southeast Atlantic region. *Atmos. Chem. Phys.*, *20*(5), 3029–3040.
https://doi.org/10.5194/acp-20-3029-2020

Kitto, M. E., & Anderson, D. L. (1988). The use of Whatman-41 filters for particle. *Atmospheric
Environment (1967)*, *22*(11), 2629–2630. https://doi.org/https://doi.org/10.1016/0004-
6981(88)90500-8

Klingebiel, M., Ghate, V. P., Naumann, A. K., Ditas, F., Pöhlker, M. L., Pöhlker, C., Kandler, K., Konow, H., & Stevens, B. (2019). Remote Sensing of Sea Salt Aerosol below Trade Wind Clouds. *Journal of the Atmospheric Sciences*, *76*(5), 1189–1202. https://doi.org/10.1175/JAS-D-18-0139.1

Konovalov, I. B., Golovushkin, N. A., Beekmann, M., & Andreae, M. O. (2021). Insights into the aging of biomass burning aerosol from satellite observations and 3D atmospheric modeling: evolution of the aerosol optical properties in Siberian wildfire plumes. *Atmospheric Chemistry and Physics*, *21*(1), 357–392. https://doi.org/10.5194/acp-21-357-2021

Kristensen, T. B., Müller, T., Kandler, K., Benker, N., Hartmann, M., Prospero, J. M., Wiedensohler, A., & Stratmann, F. (2016). Properties of cloud condensation nuclei (CCN) in the trade wind marine boundary layer of the western North Atlantic. *Atmos. Chem. Phys.*, *16*(4), 2675–2688. https://doi.org/10.5194/acp-16-2675-2016

Krueger, B. J., Grassian, V. H., Cowin, J. P., & Laskin, A. (2004). Heterogeneous chemistry of individual mineral dust particles from different dust source regions: the importance of particle mineralogy. *Atmospheric Environment*, *38*(36), 6253–6261. https://doi.org/https://doi.org/10.1016/j.atmosenv.2004.07.010

Laskin, A., Moffet, R. C., Gilles, M. K., Fast, J. D., Zaveri, R. A., Wang, B., Nigge, P., & Shutthanandan, J. (2012). Tropospheric chemistry of internally mixed sea salt and organic particles: Surprising reactivity of NaCl with weak organic acids. *Journal of Geophysical Research: Atmospheres*, *117*(D15). https://doi.org/https://doi.org/10.1029/2012JD017743

Laskin, A., Wietsma, T. W., Krueger, B. J., & Grassian, V. H. (2005). Heterogeneous chemistry of individual mineral dust particles with nitric acid: A combined CCSEM/EDX, ESEM, and ICP-MS study. *Journal of Geophysical Research: Atmospheres*, *110*(D10). https://doi.org/https://doi.org/10.1029/2004JD005206

Lathem, T. L., Beyersdorf, A. J., Thornhill, K. L., Winstead, E. L., Cubison, M. J., Hecobian, A., Jimenez, J. L., Weber, R. J., Anderson, B. E., & Nenes, A. (2013). Analysis of CCN activity of Arctic aerosol and Canadian biomass burning during summer 2008. *Atmospheric Chemistry and Physics*, *13*(5), 2735–2756. https://doi.org/10.5194/acp-13-2735-2013

Levin, Z., Teller, A., Ganor, E., & Yin, Y. (2005). On the interactions of mineral dust, sea-salt particles, and clouds: A measurement and modeling study from the Mediterranean Israeli Dust Experiment campaign. *Journal of Geophysical Research: Atmospheres*, *110*(D20). https://doi.org/https://doi.org/10.1029/2005JD005810

Li, J., Pósfai, M., Hobbs, P. v, & Buseck, P. R. (2003). Individual aerosol particles from biomass burning in southern Africa: 2, Compositions and aging of inorganic particles. *Journal of Geophysical Research: Atmospheres*, *108*(D13). https://doi.org/https://doi.org/10.1029/2002JD002310

Li, W., Shao, L., Wang, Z., Shen, R., Yang, S., & Tang, U. (2010). Size, composition, and mixing state of individual aerosol particles in a South China coastal city. *Journal of Environmental Sciences*, *22*(4), 561–569. https://doi.org/https://doi.org/10.1016/S1001-0742(09)60146-7

Maenhaut, W., Salma, I., Cafmeyer, J., Annegarn, H. J., & Andreae, M. O. (1996). Regional atmospheric aerosol composition and sources in the eastern Transvaal, South Africa, and impact of biomass burning. *Journal of Geophysical Research: Atmospheres*, *101*(D19), 23631–23650. https://doi.org/https://doi.org/10.1029/95JD02930

McCoy, D. T., Burrows, S. M., Wood, R., Grosvenor, D. P., Elliott, S. M., Ma, P.-L., Rasch, P. J., & Hartment, D. L. (2022). Natural aerosols explain seasonal and spatial patterns of Southern Ocean cloud albedo. *Science Advances*, *1*(6), e1500157. https://doi.org/10.1126/sciadv.1500157

McFiggans, G., Artaxo, P., Baltensperger, U., Coe, H., Facchini, M. C., Feingold, G., Fuzzi, S., Gysel, M., Laaksonen, A., Lohmann, U., Mentel, T. F., Murphy, D. M., O'Dowd, C. D., Snider, J. R., & Weingartner, E. (2006). The effect of physical and chemical aerosol properties on warm cloud droplet activation. *Atmospheric Chemistry and Physics*, *6*(9), 2593–2649. https://doi.org/10.5194/acp-6-2593-2006

Miles, J. C., Crutzen, P. J., & Goldammer, J. G. (1995). Fire in the Environment: The Ecological, Atmospheric and Climatic Importance of Vegetation Fires. *Journal of Ecology*, *83*, 549.

Miller, R. M., McFarquhar, G. M., Rauber, R. M., O'Brien, J. R., Gupta, S., Segal-Rozenhaimer, M., Dobracki, A. N., Sedlacek, A. J., Burton, S. P., Howell, S. G., Freitag, S., & Dang, C. (2021). Observations of supermicron-sized aerosols originating from biomass burning in southern Central Africa. *Atmos. Chem. Phys.*, *21*(19), 14815–14831. https://doi.org/10.5194/acp-21-14815-2021

Moran-Zuloaga, D., Ditas, F., Walter, D., Saturno, J., Brito, J., Carbone, S., Chi, X., de Angelis, I., Baars, H., Godoi, R. H. M., Heese, B., Holanda, B. A., Lavrič, J. v, Martin, S. T., Ming, J., Pöhlker, M. L., Ruckteschler, N., Su, H., Wang, Y., … Pöhlker, C. (2018). Long-term study on coarse mode aerosols in the Amazon rain forest with the frequent intrusion of Saharan dust plumes. *Atmospheric Chemistry and Physics*, *18*(13), 10055–10088. https://doi.org/10.5194/acp-18-10055-2018

Murphy, D. M., Cziczo, D. J., Froyd, K. D., Hudson, P. K., Matthew, B. M., Middlebrook, A. M., Peltier, R. E., Sullivan, A., Thomson, D. S., & Weber, R. J. (2006). Single-particle mass spectrometry of tropospheric aerosol particles. *Journal of Geophysical Research: Atmospheres*, *111*(D23). https://doi.org/https://doi.org/10.1029/2006JD007340

Nájera, J. J., & Horn, A. B. (2009). Infrared spectroscopic study of the effect of oleic acid on the deliquescence behaviour of ammonium sulfate aerosol particles. *Physical Chemistry Chemical Physics*, *11*(3), 483–494. https://doi.org/10.1039/B812182F

O'Dowd, C. D., & de Leeuw, G. (2007). Marine aerosol production: a review of the current knowledge. *Philosophical Transactions of the Royal Society A: Mathematical, Physical and Engineering Sciences*, *365*(1856), 1753–1774. https://doi.org/10.1098/rsta.2007.2043

O'Dowd, C. D., Facchini, M. C., Cavalli, F., Ceburnis, D., Mircea, M., Decesari, S., Fuzzi, S., Yoon, Y. J., & Putaud, J.-P. (2004). Biogenically driven organic contribution to marine aerosol. *Nature*, *431*(7009), 676–680. https://doi.org/10.1038/nature02959

Pachauri, T., Singla, V., Satsangi, A., Lakhani Anita, & Kumari, K. M. (2013). SEM-EDX Characterization of Individual Coarse Particles in Agra, India. *Aerosol and Air Quality Research*, *13*(2), 523–536. https://doi.org/10.4209/aaqr.2012.04.0095

Petters, M. D., & Kreidenweis, S. M. (2007). A single parameter representation of hygroscopic growth and cloud condensation nucleus activity. *Atmospheric Chemistry and Physics*, *7*(8), 1961–1971. https://doi.org/10.5194/acp-7-1961-2007

Pierce, J. R., Chen, K., & Adams, P. J. (2007). Contribution of primary carbonaceous aerosol to cloud condensation nuclei: processes and uncertainties evaluated with a global aerosol microphysics

model. *Atmospheric Chemistry and Physics*, *7*(20), 5447–5466. https://doi.org/10.5194/acp-7-5447-2007

Pósfai, M., Simonics, R., Li, J., Hobbs, P. v, & Buseck, P. R. (2003). Individual aerosol particles from biomass burning in southern Africa: 1. Compositions and size distributions of carbonaceous particles. *Journal of Geophysical Research: Atmospheres*, *108*(D13). https://doi.org/https://doi.org/10.1029/2002JD002291

Prospero, J. M. (1968). atmospheric dust studies on Barbados. *Bulletin of the American Meteorological Society*, *49*(6), 645–652. https://doi.org/10.1175/1520-0477-49.6.645

Prospero, J. M. (1999). Long-range transport of mineral dust in the global atmosphere: Impact of African dust on the environment of the southeastern United States. *Proceedings of the National Academy of Sciences*, *96*(7), 3396 LP – 3403. https://doi.org/10.1073/pnas.96.7.3396

Prospero, J. M., Barkley, A. E., Gaston, C. J., Gatineau, A., Campos y Sansano, A., & Panechou, K. (2020). Characterizing and Quantifying African Dust Transport and Deposition to South America: Implications for the Phosphorus Budget in the Amazon Basin. *Global Biogeochemical Cycles*, *34*(9), e2020GB006536. https://doi.org/https://doi.org/10.1029/2020GB006536

Prospero, J. M., Blades, E., Mathison, G., & Naidu, R. (2005). Interhemispheric transport of viable fungi and bacteria from Africa to the Caribbean with soil dust. *Aerobiologia*, *21*(1), 1–19. https://doi.org/10.1007/s10453-004-5872-7

Prospero, J. M., Collard, F.-X., Molinié, J., & Jeannot, A. (2014). Characterizing the annual cycle of African dust transport to the Caribbean Basin and South America and its impact on the environment and air quality. *Global Biogeochemical Cycles*, *28*(7), 757–773. https://doi.org/https://doi.org/10.1002/2013GB004802

Prospero, J. M., Delany, A. C., Delany, A. C., & Carlson, T. N. (2021). The Discovery of African Dust Transport to the Western Hemisphere and the Saharan Air Layer: A History. *Bulletin of the American Meteorological Society*, *102*(6), E1239–E1260. https://doi.org/10.1175/BAMS-D-19-0309.1

Prospero, J. M., Glaccum, R. A., & Nees, R. T. (1981). Atmospheric transport of soil dust from Africa to South America. *Nature*, *289*(5798), 570–572. https://doi.org/10.1038/289570a0

Prospero, J. M., & Lamb, P. J. (n.d.). *prospero2003*.

Prospero, J. M., & Lamb, P. J. (2003). African Droughts and Dust Transport to the Caribbean: Climate Change Implications. *Science*, *302*(5647), 1024–1027. https://doi.org/10.1126/science.1089915

Prospero, J. M., & Mayol-Bracero, O. L. (2013). Understanding the Transport and Impact of African Dust on the Caribbean Basin. *Bulletin of the American Meteorological Society*, *94*(9), 1329–1337. https://doi.org/10.1175/BAMS-D-12-00142.1

Pszenny, A., Fischer, C., Mendez, A., & Zetwo, M. (1993). Direct comparison of cellulose and quartz fiber filters for sampling submicrometer aerosols in the marine boundary layer. *Atmospheric Environment. Part A. General Topics*, *27*(2), 281–284. https://doi.org/https://doi.org/10.1016/0960-1686(93)90359-7

Quinn, P. K., Bates, T. S., Coffman, D. J., & Covert, D. S. (2008). Influence of particle size and chemistry on the cloud nucleating properties of aerosols. *Atmospheric Chemistry and Physics*, *8*(4), 1029–1042. https://doi.org/10.5194/acp-8-1029-2008

Quinn, P. K., Thompson, E. J., Coffman, D. J., Baidar, S., Bariteau, L., Bates, T. S., Bigorre, S., Brewer, A., de Boer, G., de Szoeke, S. P., Drushka, K., Foltz, G. R., Intrieri, J., Iyer, S., Fairall, C. W., Gaston, C. J., Jansen, F., Johnson, J. E., Krüger, O. O., … Zuidema, P. (2021). Measurements from the RV Ronald H. Brown and related platforms as part of the Atlantic Tradewind Ocean-Atmosphere Mesoscale Interaction Campaign (ATOMIC). *Earth Syst. Sci. Data*, *13*(4), 1759–1790. https://doi.org/10.5194/essd-13-1759-2021

Rauber, R. M., Stevens, B., Ochs, H. T., Knight, C., Albrecht, B. A., Blyth, A. M., Fairall, C. W., Jensen, J. B., Lasher-Trapp, S. G., Mayol-Bracero, O. L., Vali, G., Anderson, J. R., Baker, B. A., Bandy, A. R., Burnet, E., Brenguier, J.-L., Brewer, W. A., Brown, P. R. A., Chuang, R., … Zuidema, P. (2007). Rain in Shallow Cumulus Over the Ocean: The RICO Campaign. *Bulletin of the American Meteorological Society*, *88*(12), 1912–1928. https://doi.org/10.1175/BAMS-88-12-1912

Reid, J. S., Hobbs, P. v, Ferek, R. J., Blake, D. R., Martins, J. V., Dunlap, M. R., & Liousse, C. (1998). Physical, chemical, and optical properties of regional hazes dominated by smoke in Brazil. *Journal of Geophysical Research: Atmospheres*, *103*(D24), 32059–32080. https://doi.org/https://doi.org/10.1029/98JD00458

Reid, J. S., Koppmann, R., Eck, T. F., & Eleuterio, D. P. (2005). A review of biomass burning emissions part II: intensive physical properties of biomass burning particles. *Atmospheric Chemistry and Physics*, *5*(3), 799–825. https://doi.org/10.5194/acp-5-799-2005

Remoundaki, E., Bourliva, A., Kokkalis, P., Mamouri, R. E., Papayannis, A., Grigoratos, T., Samara, C., & Tsezos, M. (2011). PM10 composition during an intense Saharan dust transport event over Athens (Greece). *Science of The Total Environment*, *409*(20), 4361–4372. https://doi.org/https://doi.org/10.1016/j.scitotenv.2011.06.026

Roberts, G. C., Artaxo, P., Zhou, J., Swietlicki, E., & Andreae, M. O. (2002). Sensitivity of CCN spectra on chemical and physical properties of aerosol: A case study from the Amazon Basin. *Journal of Geophysical Research: Atmospheres*, *107*(D20), LBA 37-1-LBA 37-18. https://doi.org/https://doi.org/10.1029/2001JD000583

Roberts, G. C., & Nenes, A. (2005). A Continuous-Flow Streamwise Thermal-Gradient CCN Chamber for Atmospheric Measurements. *Aerosol Science and Technology*, *39*(3), 206–221. https://doi.org/10.1080/027868290913988

Roberts, G., Wooster, M. J., & Lagoudakis, E. (2009). Annual and diurnal african biomass burning temporal dynamics. *Biogeosciences*, *6*(5), 849–866. https://doi.org/10.5194/bg-6-849-2009

Rogers, C. F., Hudson, J. G., Zielinska, B., Tanner, R. L., Hallett, J., & Watson, J. G. (1991). *Cloud condensation nuclei from biomass burning*. Massachusetts Inst of Tech Press. http://inis.iaea.org/search/search.aspx?orig_q=RN:23066783

Rolph, G., Stein, A., & Stunder, B. (2017). Real-time Environmental Applications and Display sYstem: READY. *Environmental Modelling & Software*, *95*, 210–228. https://doi.org/https://doi.org/10.1016/j.envsoft.2017.06.025

Rose, D., Gunthe, S. S., Mikhailov, E., Frank, G. P., Dusek, U., Andreae, M. O., & Pöschl, U. (2008). Calibration and measurement uncertainties of a continuous-flow cloud condensation nuclei counter (DMT-CCNC): CCN activation of ammonium sulfate and sodium chloride aerosol particles in theory and experiment. *Atmospheric Chemistry and Physics*, *8*(5), 1153–1179. https://doi.org/10.5194/acp-8-1153-2008

Rosenfeld, D., Rudich, Y., & Lahav, R. (2001). Desert dust suppressing precipitation: A possible desertification feedback loop. *Proceedings of the National Academy of Sciences*, *98*(11), 5975 LP – 5980. https://doi.org/10.1073/pnas.101122798

Russell, L. M., Hawkins, L. N., Frossard, A. A., Quinn, P. K., & Bates, T. S. (2010). Carbohydrate-like composition of submicron atmospheric particles and their production from ocean bubble bursting. *Proceedings of the National Academy of Sciences*, *107*(15), 6652 LP – 6657. https://doi.org/10.1073/pnas.0908905107

Savoie, D. L., Arimoto, R., Keene, W. C., Prospero, J. M., Duce, R. A., & Galloway, J. N. (2002). Marine biogenic and anthropogenic contributions to non-sea-salt sulfate in the marine boundary layer over the North Atlantic Ocean. *Journal of Geophysical Research: Atmospheres*, *107*(D18), AAC 3-1-AAC 3-21. https://doi.org/https://doi.org/10.1029/2001JD000970

Schill, G. P., Froyd, K. D., Bian, H., Kupc, A., Williamson, C., Brock, C. A., Ray, E., Hornbrook, R. S., Hills, A. J., Apel, E. C., Chin, M., Colarco, P. R., & Murphy, D. M. (2020). Widespread biomass burning smoke throughout the remote troposphere. *Nature Geoscience*, *13*(6), 422–427. https://doi.org/10.1038/s41561-020-0586-1

Shen, H., Peters, T. M., Casuccio, G. S., Lersch, T. L., West, R. R., Kumar, A., Kumar, N., & Ault, A. P. (2016). Elevated Concentrations of Lead in Particulate Matter on the Neighborhood-Scale in Delhi, India As Determined by Single Particle Analysis. *Environmental Science & Technology*, *50*(10), 4961–4970. https://doi.org/10.1021/acs.est.5b06202

Sobanska, S., Coeur, C., Maenhaut, W., & Adams, F. (2003). SEM-EDX Characterisation of Tropospheric Aerosols in the Negev Desert (Israel). *Journal of Atmospheric Chemistry*, *44*(3), 299–322. https://doi.org/10.1023/A:1022969302107

Sobanska, S., Falgayrac, G., Rimetz-Planchon, J., Perdrix, E., Brémard, C., & Barbillat, J. (2014). Resolving the internal structure of individual atmospheric aerosol particle by the combination of Atomic Force Microscopy, ESEM–EDX, Raman and ToF–SIMS imaging. *Microchemical Journal*, *114*, 89–98. https://doi.org/https://doi.org/10.1016/j.microc.2013.12.007

Sorooshian, A., Corral, A. F., Braun, R. A., Cairns, B., Crosbie, E., Ferrare, R., Hair, J., Kleb, M. M., Hossein Mardi, A., Maring, H., McComiskey, A., Moore, R., Painemal, D., Scarino, A. J., Schlosser, J., Shingler, T., Shook, M., Wang, H., Zeng, X., … Zuidema, P. (2020). Atmospheric Research Over the Western North Atlantic Ocean Region and North American East Coast: A Review of Past Work and Challenges Ahead. *Journal of Geophysical Research: Atmospheres*, *125*(6), e2019JD031626. https://doi.org/https://doi.org/10.1029/2019JD031626

Spracklen, D. v, Carslaw, K. S., Pöschl, U., Rap, A., & Forster, P. M. (2011). Global cloud condensation nuclei influenced by carbonaceous combustion aerosol. *Atmospheric Chemistry and Physics*, *11*(17), 9067–9087. https://doi.org/10.5194/acp-11-9067-2011

Stein, A. F., Draxler, R. R., Rolph, G. D., Stunder, B. J. B., Cohen, M. D., & Ngan, F. (2015). NOAA's HYSPLIT Atmospheric Transport and Dispersion Modeling System. *Bulletin of the American Meteorological Society*, *96*(12), 2059–2077. https://doi.org/10.1175/BAMS-D-14-00110.1

Stevens, B., Bony, S., Farrell, D., Ament, F., Blyth, A., Fairall, C., Karstensen, J., Quinn, P. K., Speich, S., Acquistapace, C., Aemisegger, F., Albright, A. L., Bellenger, H., Bodenschatz, E., Caesar, K.-A., Chewitt-Lucas, R., de Boer, G., Delanoë, J., Denby, L., … Zöger, M. (2021). EUREC4A. *Earth Syst. Sci. Data*, *13*(8), 4067–4119. https://doi.org/10.5194/essd-13-4067-2021

Stevens, B., Farrell, D., Hirsch, L., Jansen, F., Nuijens, L., Serikov, I., Brügmann, B., Forde, M., Linne, H., Lonitz, K., & Prospero, J. M. (2016). The Barbados Cloud Observatory: Anchoring Investigations of Clouds and Circulation on the Edge of the ITCZ. *Bulletin of the American Meteorological Society*, *97*(5), 787–801. https://doi.org/10.1175/BAMS-D-14-00247.1

Talbot, R. W., Andreae, M. O., Berresheim, H., Artaxo, P., Garstang, M., Harriss, R. C., Beecher, K. M., & Li, S. M. (1990). Aerosol chemistry during the wet season in central Amazonia: The influence of long-range transport. *Journal of Geophysical Research: Atmospheres*, *95*(D10), 16955–16969. https://doi.org/https://doi.org/10.1029/JD095iD10p16955

Tomlin, J. M., Jankowski, K. A., Veghte, D. P., China, S., Wang, P., Fraund, M., Weis, J., Zheng, G., Wang, Y., Rivera-Adorno, F., Raveh-Rubin, S., Knopf, D. A., Wang, J., Gilles, M. K., Moffet, R. C., & Laskin, A. (2021). Impact of dry intrusion events on the composition and mixing state of particles during the winter Aerosol and Cloud Experiment in the Eastern North Atlantic (ACE-ENA). *Atmospheric Chemistry and Physics*, *21*(24), 18123–18146. https://doi.org/10.5194/acp-21-18123-2021

Tsamalis, C., Chédin, A., Pelon, J., & Capelle, V. (2013). The seasonal vertical distribution of the Saharan Air Layer and its modulation by the wind. *Atmos. Chem. Phys.*, *13*(22), 11235–11257. https://doi.org/10.5194/acp-13-11235-2013

Twohy, C. H., Kreidenweis, S. M., Eidhammer, T., Browell, E. v., Heymsfield, A. J., Bansemer, A. R., Anderson, B. E., Chen, G., Ismail, S., DeMott, P. J., & van den Heever, S. C. (2009). Saharan dust particles nucleate droplets in eastern Atlantic clouds. *Geophysical Research Letters*. https://doi.org/10.1029/2008GL035846

Twomey, S. (1974). Pollution and the planetary albedo. *Atmospheric Environment (1967)*, *8*(12), 1251–1256. https://doi.org/https://doi.org/10.1016/0004-6981(74)90004-3

Twomey, S. (1977). The Influence of Pollution on the Shortwave Albedo of Clouds. *Journal of Atmospheric Sciences*, *34*(7), 1149–1152. https://doi.org/10.1175/1520-0469(1977)034<1149:TIOPOT>2.0.CO;2

Wang, Q., Saturno, J., Chi, X., Walter, D., Lavric, J. v, Moran-Zuloaga, D., Ditas, F., Pöhlker, C., Brito, J., Carbone, S., Artaxo, P., & Andreae, M. O. (2016). Modeling investigation of light-absorbing aerosols in the Amazon Basin during the wet season. *Atmospheric Chemistry and Physics*, *16*(22), 14775–14794. https://doi.org/10.5194/acp-16-14775-2016

Wex, H., Dieckmann, K., Roberts, G. C., Conrath, T., Izaguirre, M. A., Hartmann, S., Herenz, P., Schäfer, M., Ditas, F., Schmeissner, T., Henning, S., Wehner, B., Siebert, H., & Stratmann, F. (2016). Aerosol arriving on the Caribbean island of Barbados: physical properties and origin. *Atmos. Chem. Phys.*, *16*(22), 14107–14130. https://doi.org/10.5194/acp-16-14107-2016

1062 Wu, H., Taylor, J. W., Langridge, J. M., Yu, C., Allan, J. D., Szpek, K., Cotterell, M. I., Williams, P. I.,
1063   Flynn, M., Barker, P., Fox, C., Allen, G., Lee, J., & Coe, H. (2021). Rapid transformation of
1064   ambient absorbing aerosols from West African biomass burning. *Atmospheric Chemistry and*
1065   *Physics*, *21*(12), 9417–9440. https://doi.org/10.5194/acp-21-9417-2021

1066 Yu, H., Tan, Q., Chin, M., Remer, L. A., Kahn, R. A., Bian, H., Kim, D., Zhang, Z., Yuan, T., Omar, A.
1067   H., Winker, D. M., Levy, R., Kalashnikova, O., Crepeau, L., Capelle, V., & Chedin, A. (2019).
1068   Estimates of African Dust Deposition Along the Trans-Atlantic Transit Using the Decade-long
1069   Record of Aerosol Measurements from CALIOP, MODIS, MISR, and IASI. *Journal of Geophysical*
1070   *Research. Atmospheres : JGR*, *124*(14), 7975–7996. https://doi.org/10.1029/2019JD030574

1071 Zauscher, M. D., Wang, Y., Moore, M. J. K., Gaston, C. J., & Prather, K. A. (2013). Air Quality Impact
1072   and Physicochemical Aging of Biomass Burning Aerosols during the 2007 San Diego Wildfires.
1073   *Environmental Science & Technology*, *47*(14), 7633–7643. https://doi.org/10.1021/es4004137

1074 Zhang, R., Khalizov, A. F., Pagels, J., Zhang, D., Xue, H., & McMurry, P. H. (2008). Variability in
1075   morphology, hygroscopicity, and optical properties of soot aerosols during atmospheric processing.
1076   *Proceedings of the National Academy of Sciences*, *105*(30), 10291–10296.
1077   https://doi.org/10.1073/pnas.0804860105

1078 Zuidema, P., Alvarez, C., Kramer, S. J., Custals, L., Izaguirre, M., Sealy, P., Prospero, J. M., & Blades, E.
1079   (2019). Is Summer African Dust Arriving Earlier to Barbados? The Updated Long-Term In Situ
1080   Dust Mass Concentration Time Series from Ragged Point, Barbados, and Miami, Florida. *Bulletin of*
1081   *the American Meteorological Society*, *100*(10), 1981–1986. https://doi.org/10.1175/BAMS-D-18-
1082   0083.1

1083 Zuidema, P., Sedlacek III, A. J., Flynn, C., Springston, S., Delgadillo, R., Zhang, J., Aiken, A. C.,
1084   Koontz, A., & Muradyan, P. (2018). The Ascension Island Boundary Layer in the Remote Southeast
1085   Atlantic is Often Smoky. *Geophysical Research Letters*, *45*(9), 4456–4465.
1086   https://doi.org/https://doi.org/10.1002/2017GL076926

1087 Zuidema, P., Xue, H., & Feingold, G. (2008). Shortwave Radiative Impacts from Aerosol Effects on
1088   Marine Shallow Cumuli. *Journal of the Atmospheric Sciences*, *65*(6), 1979–1990.
1089   https://doi.org/10.1175/2007JAS2447.1

1090

1091